PV cell impedance requirements for inductor-less power optimizers

Andreas Chourzamanis

4746457

PV cell impedance requirements for inductor-less power optimizers

By

Andreas Chourzamanis

in partial fulfilment of the requirements for the degree of

Master of Science

in Electrical Engineering

at the Delft University of Technology,

to be defended publicly on Thursday December 23, 2021 at 9:30 AM.

Supervisor:	Dr. Patrizio Manganiello
Thesis committee:	Prof. dr. Arno Smets, TU Delft
	Dr. Milos Cvetkovic TU Delft
	Dr. Patrizio Manganiello TU Delft

TU Delft

Contents

Abstract

Renewable energy sources and in particular solar energy represent our mean to mitigate global warming and reduce the dependency from fossil fuel. Also, photovoltaic panels allow for production of clean energy anywhere, also in the urban environment where, unfortunately, non-ideal working conditions such as partial shading happen often and can reduce the performance of the photovoltaic panels. To maximize the energy produced by these panels, new solutions are proposed where DC-DC converters are attached to the panel. This fact makes the system more complex, due to the necessary extra components, and add losses and volume especially from the inductor of the DC-DC converter.

In this study, a different approach has been studied to facilitate integration of DC-DC converter in photovoltaic panels. Photovoltaic cells as semiconductor devices have an intrinsic capacitance. Moreover, the metallization of the cell, especially on the back, can be redesigned to increase its inductance. Therefore, solar cells can in theory be redesigned to manipulate their output impedance and this impedance could replace the input filter of the DC-DC converter that is used to control the operating point of the photovoltaic panel. This will enable the design of novel solar modules whose operating point is controllable through inductor-less power converters.

To determine the values of the capacitance, inductance and resistance that a photovoltaic cell should have so as to allow inductor-less power conversion as efficient as in a conventional solution with module-level power optimizers, a model of a photovoltaic panel that uses one or more of these “special” cells has been developed. Simulations have been done for a single solar cell and for a photovoltaic module of 96 solar cells. The simulation results provide information for the values of ripples and efficiency of the system so as to determine values of the capacitance, inductance, and resistance of the special cells to replace the components of the converter and also the number of such cells that a PV module should have. Comparison with conventional systems is also performed to compare it with the proposed solution.

Acknowledgements

I would like to express my gratitude to my Supervisor Prof. Dr. Patrizio Manganiello for giving me this work. Also, I want to appreciate him for the excellent supervising on the progress of this work. I would like also tothank him for the encouragement he gave me throughout the time of this master thesis.

I would like to express my appreciation to my parents for encouraging me from the begging of this Msc programme until the end of my master thesis.

Chapter 1 : Introduction

Since the industrial revolution the energy consumption has started to raise and in the last 50 years the demand has sharply increased. The population of the planet has grown and most of the applications need high amounts of energy (mostly electrical). In Figure 1.1 the global energy consumption over the years is presented.

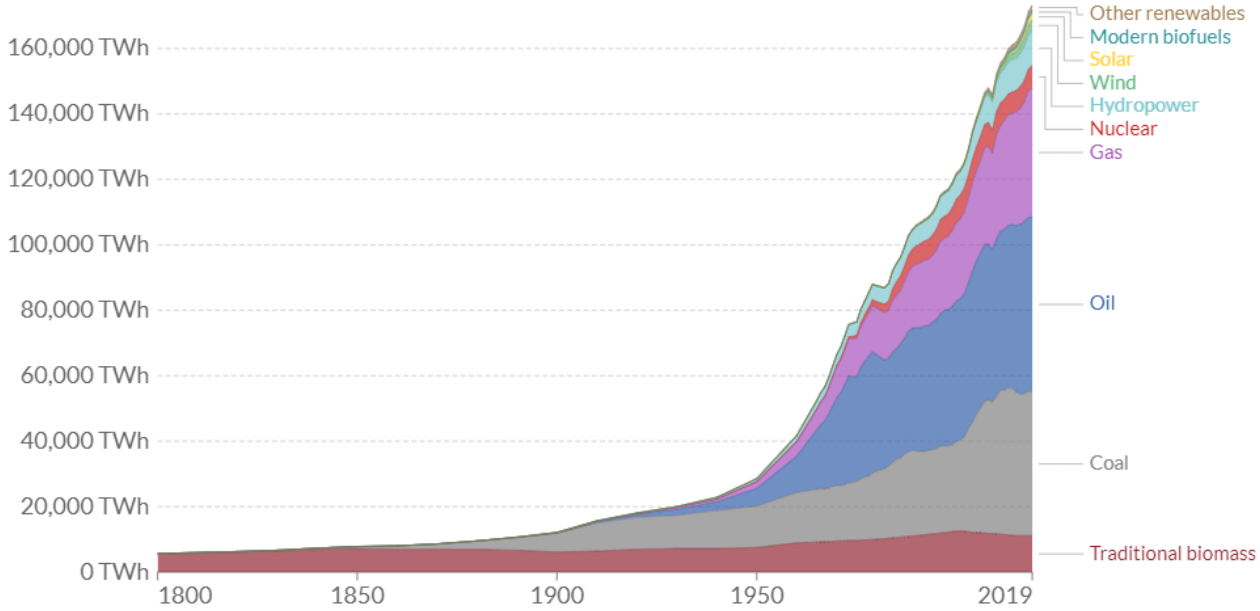

Figure 1.1: Global energy consumption over the last 200 years.[1]

The most used sources of energy after the industrial revolution were coal and oil. After several studies scientists discovered that the pollution of the air (especially in urban areas) and the greenhouse effect above the normal limit are caused by the emissions due to the consumption of these sources. The greenhouse effect is the process where the radiation from the atmosphere of the Earth heats the surface. CO_2 ,CO and CH_4 are the main greenhouse gases which means that their emissions have the highest impact on the environment, while the CO_2 is considered to be the most influential for the greenhouse effect and the rise of the planet temperature. In Figure 1.2 the greenhouse gas emissions of CO_2 from the conventional types of energy sources (coal, oil, gas etc.) are shown. Carbon dioxide interferes with infrared waves, absorbs energy, and re-emits the energy to the Earth. Almost half of the absorbed energy is re-emitted.

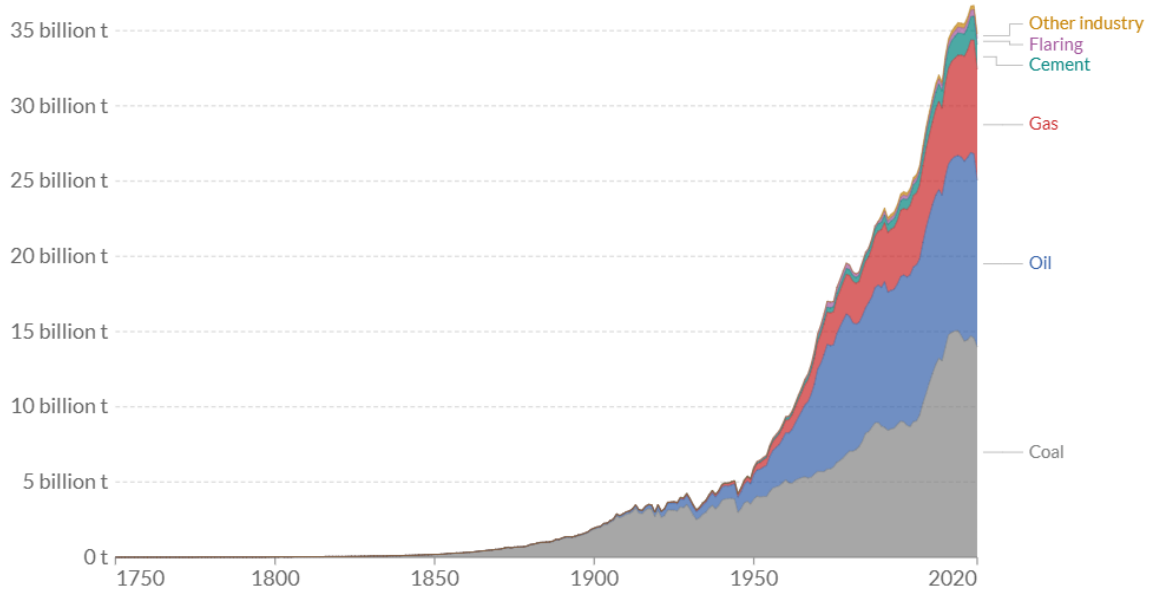

Figure 1.2: CO2 emissions from conventional types of energy.[2]

With the goal of reducing pollution, greenhouse gas emission and climate change due to global warming, renewable energy, that is generated from renewable resources such as sun, wind and water, represent a valuable alternative to coal, oil and gas. Over the last years photovoltaics is getting much attention since technology developments are leading to higher and higher efficiency and durability whereas the cost of PV energy keeps decreasing year by year, making photovoltaic the cheapest source of electricity in history [3]. In Figure 1.3 the installed capacity and the cost of photovoltaics in world is shown.

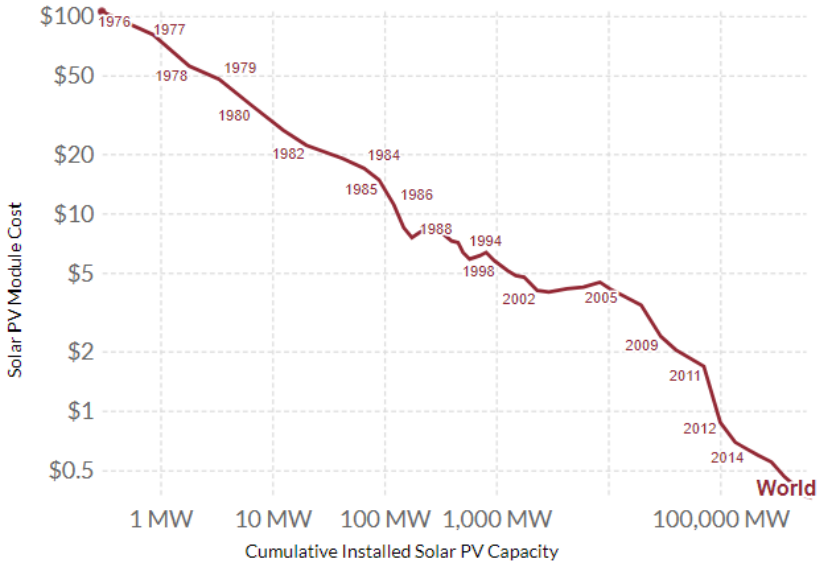

Figure 1.3: Installed capacity and price of photovoltaics over the years.[4]

In addition to the research in photovoltaics, significant attention has been given in the field of power electronics for photovoltaic application. A solar cell can provide low amounts of power, so PV cells are usually connected in series to form PM modules so as to increase the operating voltage. In addition, the provided power is affected by the irradiance that the sun is providing every time and that is fluctuating and affects the values of the current and voltage of the PV module, while this can cause several problems to the electrical system that is connected to the module. An example of such a problem can be that the PV module cannot meet the power demand or can provide power that is above the limit of the components of the system. These problems can be eliminated with the use of power electronics, as they are able of handling all the changes in voltage and current of the PV. Power electronics like inverters to transform the DC power to AC, converters to upscale or downscale the values of DC voltage and current, maximum power point trackers and any other components of a system play a role in the general performance and efficiency [5]. With the use of power electronics, power that is produced from a PV cell can be used effectively. A solar cell of the PV module performs in several values of current and voltage based on the irradiance and operating temperature. The operating point that produces the highest amount of power is called Maximum Power Point (MPP). Every PV cell or PV module should be working on its maximum power point in order to maximize the power that is produced. Maximum power point trackers ensure that the PV generator works at this point[6]. Furthermore, in the PV module several types of losses occur (they are discussed in Chapter 2). Some of these losses, for instance the mismatch losses due to partial shading can be effectively mitigated with the use of power electronics. A PV module has several solar cells connected in series, which means that the current that flows through them is equal. If a shade occurs to one cell (partial shading) or to several cells in series, either the current that flows through the PV module will be decreased or the shaded cell will be reverse-biased and start to dissipate energy from the rest of the system. In both cases, the total power of the PV module will be lowered. A typical solution for reducing the losses caused due to partial shading is to connect bypass diodes in the strings of solar cells wired in series. The bypass diode will bypass the shaded cell and prevent reverse breakdown; therefore, the losses will be reduced. The Figure 1.3 shows an example of this situation. In this example a PV module made of 6 solar cells is partially shaded (one cell is shaded) and the I-V curve is presented. The difference in the amount of power that is lost is significant. Bypass diode allows the current of the unshaded cells to flow without being limited by the shaded cell, and the PV string works as it has 5 solar cells. As it is referred above, in conventional PV modules bypass diodes are connected in anti-parallel to groups of 20-24 cells and not in parallel to each cell. [7]

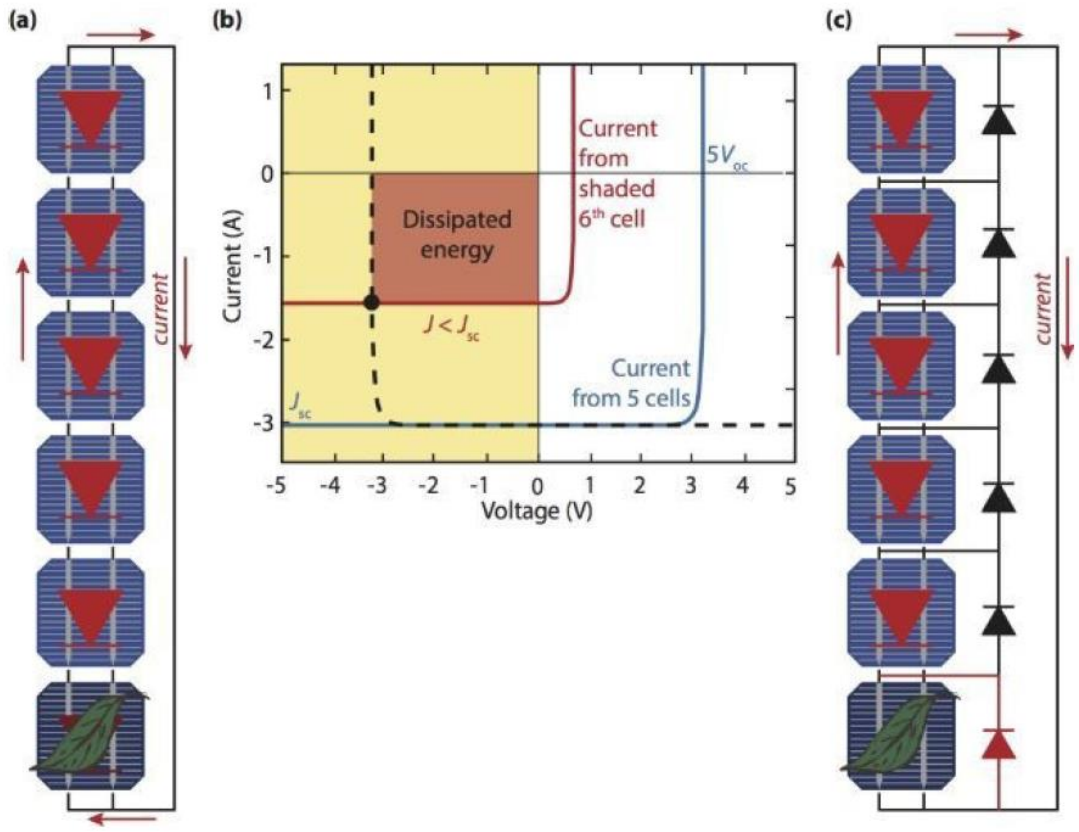

Figure 1.3: PV module under partial shading without bypass diodes and with bypass diodes.[7]

For instance, in a common PV module of 60 solar cells one bypass diode is connected in anti-parallel to every 20 cells. As it is explained above, the bypass diode will block the current of the group of solar cells that it is connected to when shading occurs and thus, the other PV strings can work at their MPP. However, even with the bypass diodes, losses can still be high. In a situation where in a group of 20 cells in series only one solar cell is shaded, the use of bypass diodes will result in blocking the whole group and therefore, a high amount of power will be lost [7].

PV systems are made of several PV modules that are connected in series and form PV strings and several PV strings are connected to form a PV array , as shown in Figure 1.4.

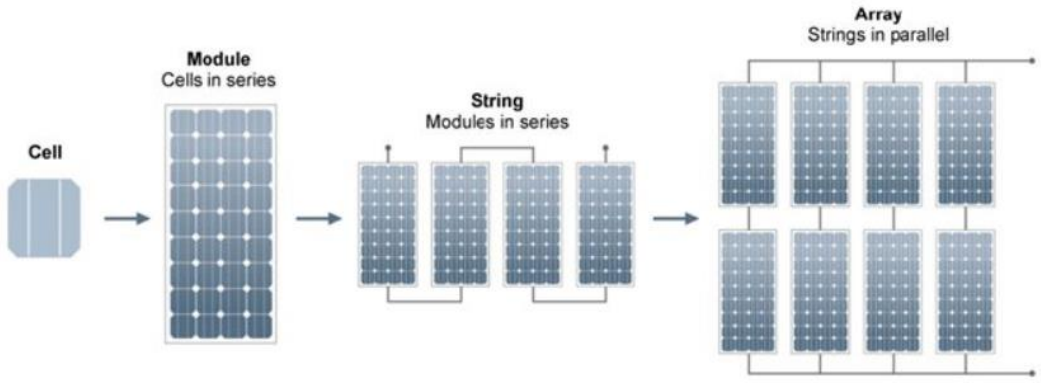

Figure 1.4: Figure 1.4: Different types of PV generators: from a single PV cell to a PV system.[8]

A PV module that is partially shaded limits the current of the whole PV string and increases the losses of the system since only the unshaded part can work at the MPP. Consequently, losses will be even higher in the whole PV array where PV strings are connected. A block diagram of a PV system is presented in Figure 1.5. Usually, each PV string of the PV array is connected to an inverter that is used to make the system work at its MPP, implementing the so-called Maximum Power Point Tracking (MPPT). In centralized solutions, that work well in open field installations, a whole PV array is connected to the inverter. In the urban environments where the effect of shading is more frequent PV systems face severe losses. This means that commercial PV modules produce less energy compared to the PV power plants outside the cities.

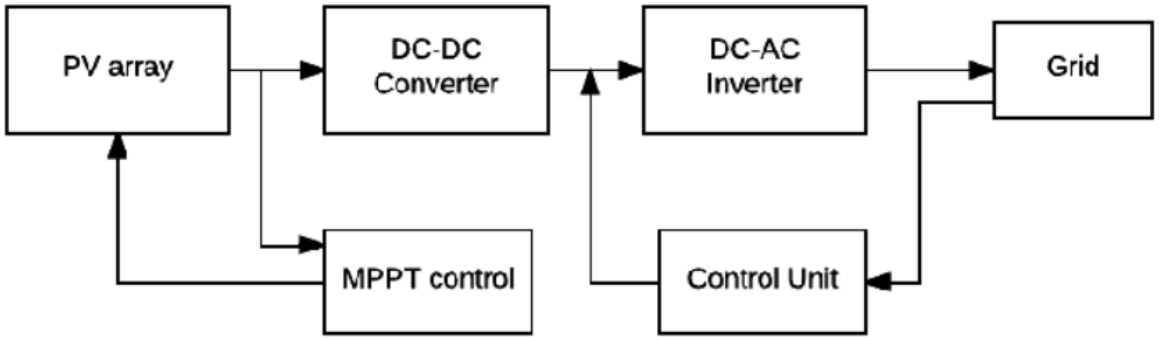

Figure 1.5: Block diagram of a PV system.[9]

Based on these factors and other such as the stability of the system, companies did research over the last years on integrating power electronic components in module of sub-module level. This means that the control of the power is done in each PV module or even in a part of it. Module level control is mostly referred as PV optimizer or module integrated converter (MIC). Taking this into account, MPPT can be performed at module level which can increase the system efficiency significantly and each module will not affect the performance of the other modules.

In Figure 1.6(a), a conventional solution is shown where a PV string is connected to a string inverter. In Figure 1.6(b) instead, every module is connected to an inverter, also called micro-inverter. Finally, in Figure 1.6(c) PV modules are connected with DC-DC converters, also known as power optimizers, to a string inverter. In Figure 1.6 concepts (b) and (c) that are related to the module level result in a better performance of the system [8]. The other concept that has been mentioned above is the sub-module level control. In this case PV optimizers will control groups of solar cells in each PV module. This can limit even more the effect of partial shading, since groups of cells are controlled with a DC-DC converter rather than getting bypassed using bypass diodes. In Figure 1.7 an example of sub-module control is shown.

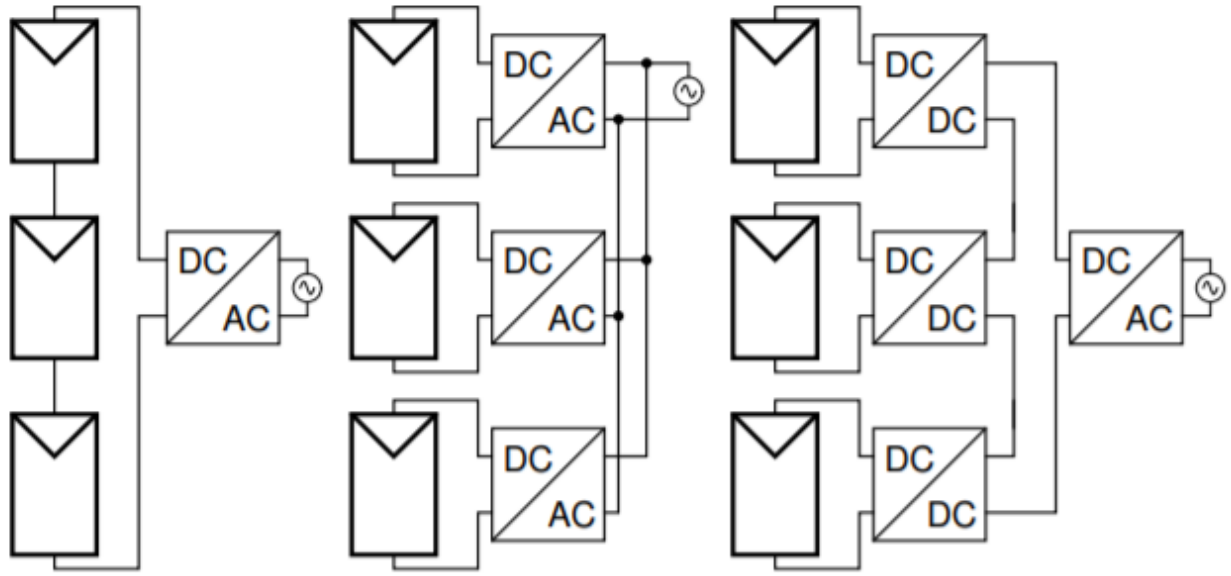

(a) Series string architecture. (b) Micro-inverter architecture. (c) Cascaded dc-dc (dc-dc optimizer) architecture.

Figure 1.6: Different PV system's architectures.[10]

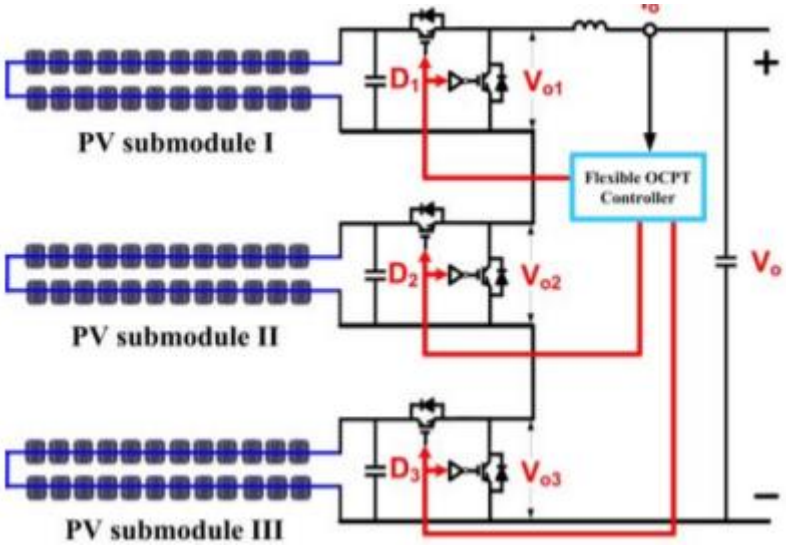

Figure 1.7: Sub-module control of a PV module.[11]

According to [11], submodule integrated converters (subMICs) with MPPTs can lead to better performance compared to the classic way of by-pass diodes, especially in mismatch situations such as partial shading. To be more specific, in some mismatch conditions subMICs can provide 30% more power based on simulation results. In Figure 1.8 there is an example of such a case that shows the power that is lost.

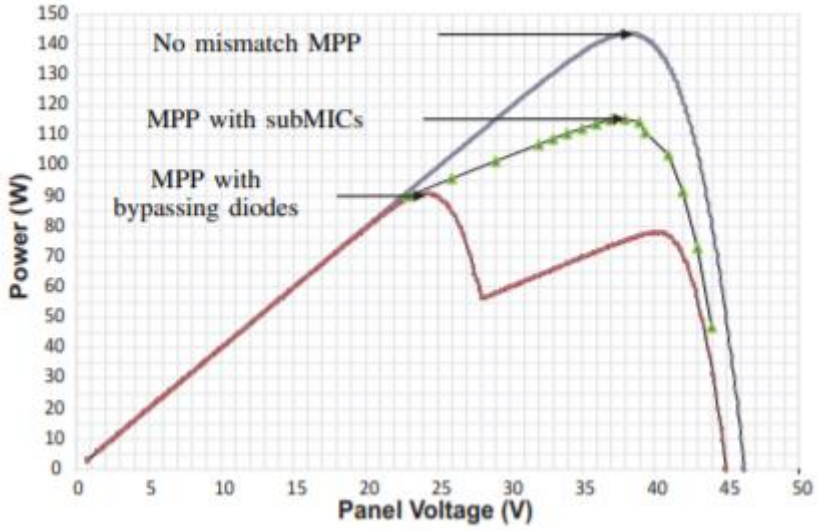

Figure 1.8: Comparison of PV modules with bypass diodes and subMICs.[12]

Another example of such a comparison is shown in Figure 1.9 and Figure 1.10 where partial shading occurs in a PV module. It shows the difference at the output power in case of sub-module PV optimizers with or without distributed MPPT. The increase in the power output is around 24%.

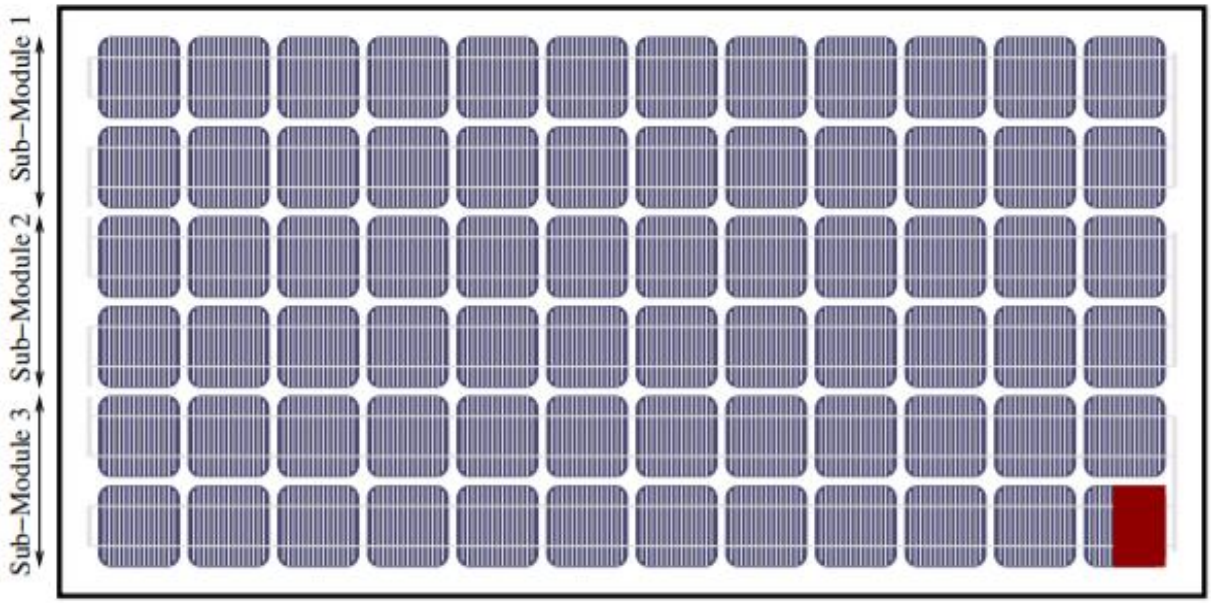

Figure 1.9: Partial shading situation.[13]

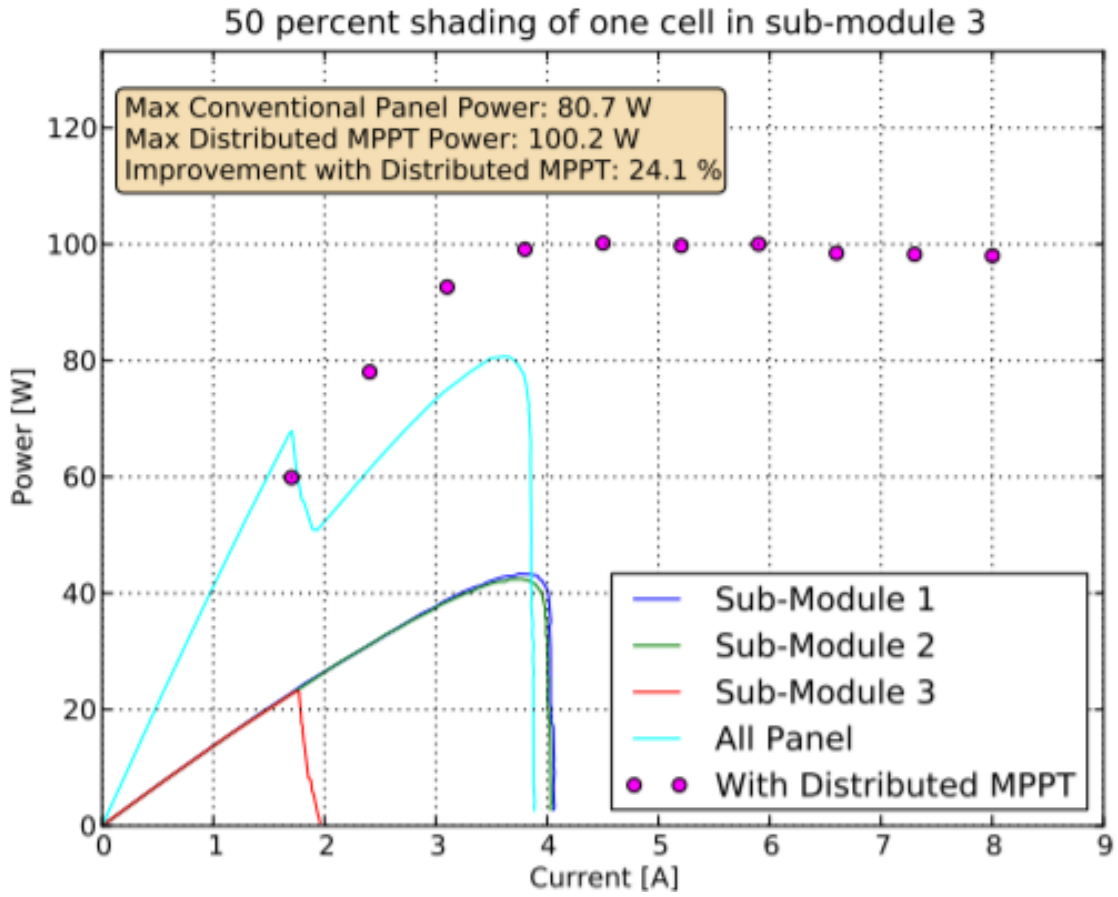

Figure 1.10: Difference in the power output of a PV module in a case of partial shading with PV optimizers in every sub-module and without.[13]

There are many companies such as Solar edge [14], Taylor Solar [15], Zerun [16] and Maxim Integrated [17] that work on the field of module and submodule power optimizers. In Figure 1.11, an example of the comparison between a PV module with only one power optimizer with bypass diodes and a PV module where there are power optimizers in every sub-module is given. In this example the power from the third sub-module that is partially shaded is lost and the sub-module consumes power from the system when module-level optimization is done. In the case of the submodule-level PV optimizers the third sub-module does not provide the system with the maximum power which is 85W, but it still provides 40W. The difference in the power that is lost is high and concerning the fact that in other situations there are many PV modules, the power that is lost can be even higher with the bypass diodes.

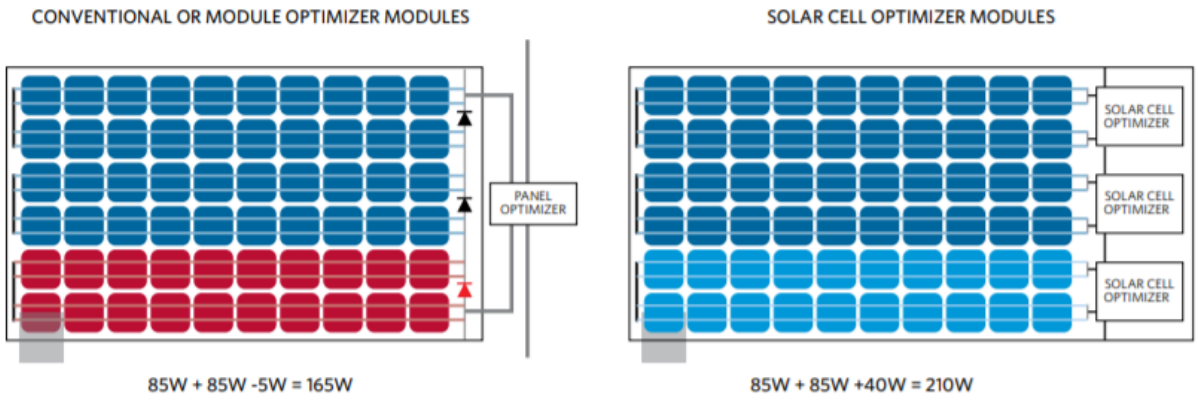

Figure 1.11: Output power comparison between one power optimizer with bypass diodes and power optimizers for each sub-module for a partial shading case.[18]

PV modules that have module or sub-module control as shown in previous examples can have significant energy harvest and reduced power degradation. In addition to this, the PV system will be reliable in delivering the necessary power as it will not be affected so much compared with the cases of the bypass diodes. Moreover, a flexibility in designing based on the needs of the application that the system will be used is another advantage because better control of the current and the voltage can be achieved. Power optimizers for each module or sub-module will be much smaller than the ones that handle the power of the whole PV module or the whole PV string. This is another argument for the flexibility of the general system. The conventional converters that are used in module-level power electronics have big components, such as the inductor of DC-DC converter that is shown in Figure 1.12. In urban applications for PV, there is usually an area limitation as the system is not set in open fields. With smaller power optimizers higher levels of flexibility can be achieved.

Figure 1.12: Example of power optimizer.[19]

1.2 Problem Statement

The increasing switching frequency of power converters, that is expected due to deployment of wide bandgap semiconductor devices, is paving the way toward converters' full integration. However, as shown previously, some components such as inductors are still too big to be integrated with ease. According to the level of power that has to be controlled the size of the converter will be increased or decreased respectfully to the power level. An ideal scenario would be to integrate these bulky passive components on the solar cells. Metallization of the solar cell can be option for achieving the necessary inductance. In addition, solar cell as a semiconductor device exhibits a capacitive behavior that can be exploited. Therefore, solar cells can in theory be redesigned to manipulate their output impedance; as shown in the following chapters, this impedance could replace the input filter of the DC-DC converter that is used to control the operating point of the PV module. This will enable the design of novel PV modules whose operating point is controllable through inductor-less power converters.

The research objective of this work is to determine the values of the capacitance, inductance and resistance that a PV cell should have so as to allow inductor-less power conversion as efficient as in a conventional solution with module-level power optimizers (based on a boost topology).

The research questions that will be answered are:

- Which ranges of PV cell impedance are acceptable so as to replace the input inductor and capacitor of boost converter?
- How can the change in the level of output voltage affect the performance of the proposed system?
- What configuration of PV cell can achieve better perfomance?
- Does the proposed system have higher efficiency and better perfomance compared to conventional PV and power optimizer system?

1.3 Thesis Outline

The outline of the current thesis is the following:

In **Chapter 2**, the equivalent circuit of a PV cell and its mathematical model are analysed. More specifically, the physics principles of a solar cell are shown for deeper understanding of the model. In addition, the losses that occur in a solar cell and the inductive and capacitive behaviour of it are presented.

In **Chapter 3**, an introduction to the inductor-less power conversion in solar cells is presented. The model of the dynamic resistance of the solar cell is analysed. Also, the mathematical model for the state space averaging and ripple of the proposed system is presented. The differential equations that govern the model are shown and solved and the physics behind the results is explained.

In **Chapter 4**, results of MATLAB simulations based on the mathematical models are presented and discussed. Figures and tables of the results are shown and interpreted in order to answer the research questions.

In **Chapter 5**, discussion and conclusions based on the simulation results are reported. Lastly, future work for the continuation of this research project is presented.

Chapter 2: Equivalent circuit model of solar cell

2.1 Solar cell working principle

A photovoltaic cell consists of two semiconductor materials that form a junction. A semiconductor junction is consisted of two semiconductor materials that are joined together. In solar cells this junction is usually a p-n junction. This means that one material is made to have excess holes and be positive (p) and the other is made to have excess electrons and be negative (n). The working principle of a solar cell is based on the photovoltaic effect. Photovoltaic effect is the generation of potential difference at the junction of the cell in response to electromagnetic radiation. This effect is closely related to the photoelectric effect as the radiation is absorbed from the semiconductor and the bonds of holes and electrons are broken.[5]

Photovoltaic cells can be made with different semiconductor materials, but these materials have different energy band gaps. Bandgap of a specific material is the minimum energy that is needed to excite an electron that is stacked in a bound to a free state . Only when the energy of the incident photons is equal or higher than the bandgap of the semiconductor material of the solar cell photons can be absorbed. The energy of the photon is given by:

$$E = hv \tag{2.1}$$

Where h is Planck's constant and v is the frequency of the photon.

Photovoltaic effect consists of three basic processes:

1. Charge carriers are generated due to the absorption of light. This means that electrons are excited from valence band to the conduction band. In other words, they are excited to a higher energy level. The energy that is needed so that electrons are excited in conduction band is dependent on the bandgap of the material. In Figure 2.1 an example of a photon absorption is shown.

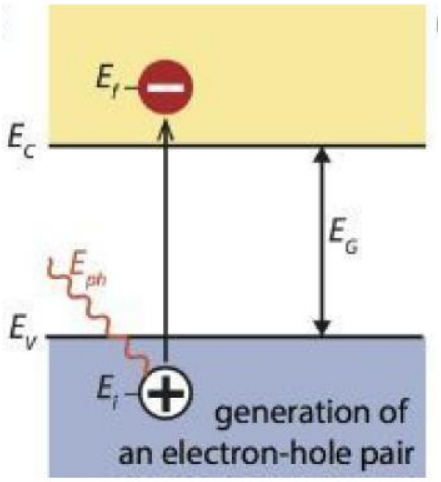

Figure 2.1: Absorption of a photon in a semiconductor.[7]

2. Separation of these photogenerated carriers. In the semiconductors, electrons and holes recombine after their bonds break, so in order to use the energy of an electron hole-pair an external circuit must be used to have flow of these charge carriers. A simple solar cell model is shown in the Figure 2.2.

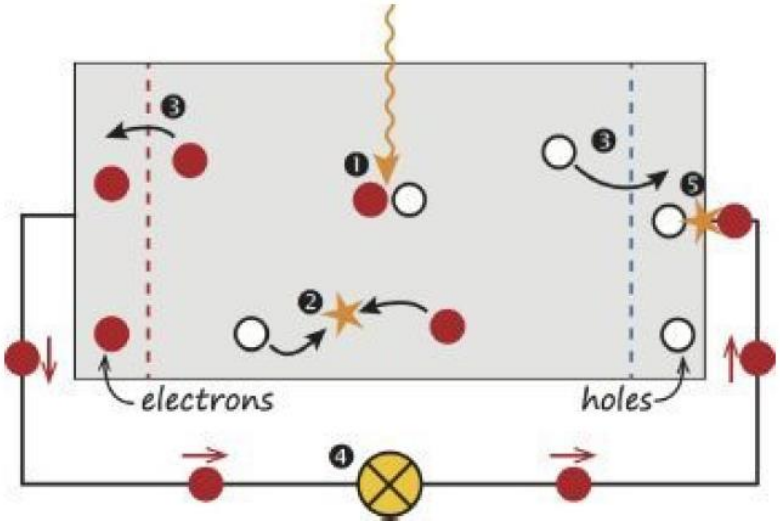

Figure 2.2: Simple solar cell model.[7]

3. Collection of these carriers at the terminals. The charge carriers are collected from the external circuit in order to be used as electric energy. After the collection, electrons recombine with holes at a metal absorber interface that is shown in Figure 2.2 (number 5) [7].

Different types of losses occur in a solar cell. The major ones are listed below:

1. Thermalization losses
2. Below bandgap losses
3. Other losses (optical losses, solar cell collection losses)

Solar cells are made of certain semiconductor materials. As it is described above, radiation is absorbed and bonds of electrons and holes break. Depending on the material of the semiconductor certain range of radiation is absorbed from the solar cell so as to break the bonds (must be higher than the bandgap of the material). When the radiation has lower energy, it cannot be absorbed from the cell and when the radiation has higher energy, excess energy is provided to the cell that is not absorbed efficiently and is released as heat. The limit in the efficiency of a solar cell is mostly referred at the Shockley-Queisser limit and is illustrated in Figure 2.3.[5]

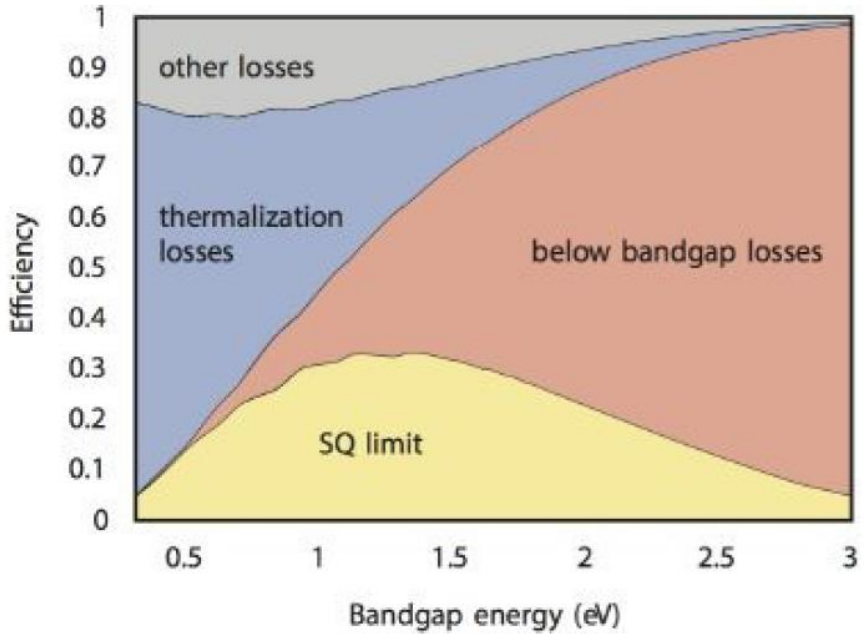

Figure 2.3: Basic loss mechanisms of solar cells.[5]

Another phenomenon that affects the operation of the photovoltaic is the so-called recombination. Recombination is mostly dependent on the defects of the material and the doping level. The basic types of recombination in semiconductors are:

1. Direct recombination
2. Shockley-Read-Hall recombination
3. Auger recombination
4. Surface recombination

Recombination is the process where excess electrons recombine with excess holes that are generated from the break of the bond and therefore, this limits the produced current of the solar cell. Direct recombination, Shockley-Read-Hall recombination and Auger recombination are mostly done in the bulk of the semiconductors. In silicon solar cells that are mostly used, the main recombination process is Auger recombination. On the other hand, surface recombination happens in the surface of the semiconductors. For example, at a silicon surface many valence electrons are not able to find a partner to make a covalent bond and they create a dangling bond which is a defect. Defects in semiconductors create states between valence and conduction band that will enhance recombination. Figure 2.4 illustrates this situation. [7]

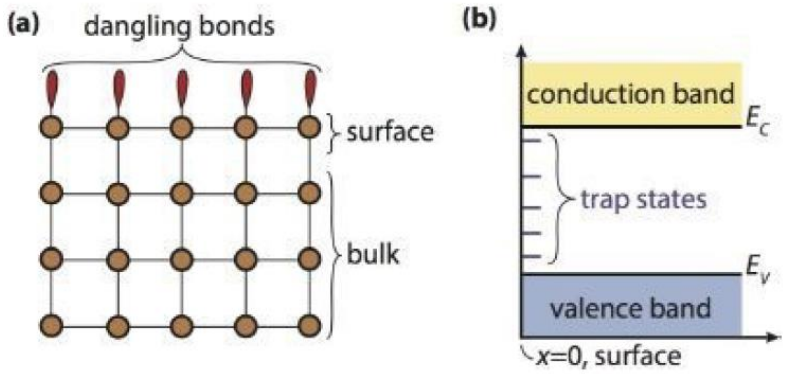

Figure 2.4: Creation of dangling bonds in semiconductors.[5]

It is important to introduce the term of depletion region. Depletion region is the area between the p-n junction (metallurgical junction) that is depleted of mobile charge carriers (electrons and holes) due to the diffusion process. Diffusion process is the process when the excess holes from p-semiconductor and excess electrons from n-semiconductor cause a diffusion current in the metallurgical junction. The region acts as a barrier for the current to flow as it creates an internal electric field.[14]

As mentioned before, solar cells, behave similar to semiconductor diodes and this means that they have also a capacitive behaviour. In semiconductor junctions there is an area that is called depletion region where there are separated charge carriers and these carriers add this capacitive property. In Figure 2.6 the depletion region of a p-n junction is shown.

Capacitance is defined as:

$$C = \frac{dQ}{dV} \tag{2.2}$$

This capacitance in a semiconductor can be divided in junction capacitance and diffusion capacitance. Junction capacitance is mostly dependent on the charge modulation in the depletion region and the diffusion capacitance is dependent on the stored charges in the depletion region. The equation 2.2 shows that the capacitance is dependent on the change of charges in the depletion region and the change in the applied voltage. The depletion region of the junction acts as a dielectric medium that stores charges. The stored charges in the depletion region determine the capacitance of the junction. When reverse-biased voltage is applied, the depletion region width increases (as it enhances an opposite electric field) but the width of p and n regions decrease, so less charges are stored. This leads to lower capacitance.[20]

Under illumination the depletion area decreases while the bonds of electrons and holes break and the density of them near the depletion region is higher. Current flows through the diode and the diffusion capacitance increases. As it is explained in the photovoltaic effect working principle, absorbed irradiation creates electron-hole pairs and thus, these pairs will also be created in the depletion region and produce a photocurrent, as shown in Figure 2.5. When the solar cell is connected to a load, the produced photocurrent creates a voltage drop to the

load so that current flows. This leads to a forward biased situation to the semiconductor junction [20].

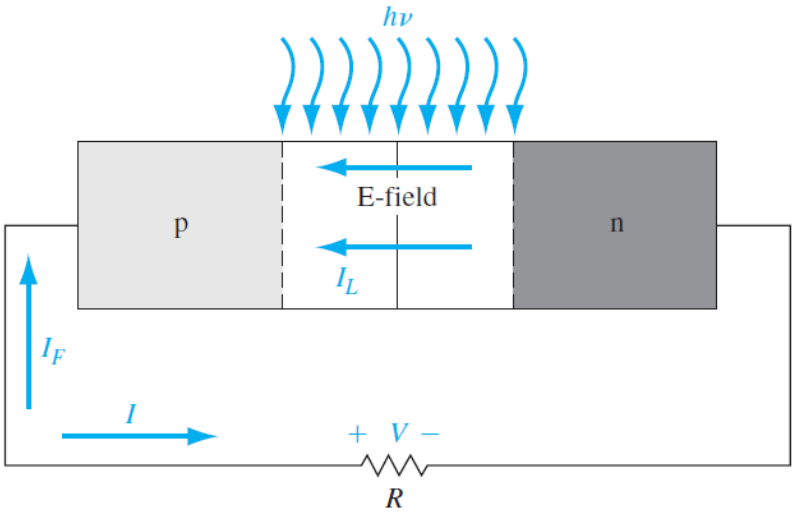

Figure 2.5: Solar cell under illumination.[20]

So capacitive behaviour is intrinsic to the solar cell. A p-n junction under illumination has the same behaviour as if it is at forward bias mode that is shown in Figure 2.6(c). As shown in Figure 2.6, the depletion region width W is smaller in forward biased mode (c) compared to the thermal equilibrium case (a). The diffusion capacitance is given by the equation:

$$C_d = \frac{q^2 ni^2 A}{2kT}\left(\frac{\sqrt{D_{p0}\tau_{p0}}}{N_d} + \frac{\sqrt{D_{n0}\tau_{n0}}}{N_a}\right) e^{\frac{qV_a}{kT}} \tag{2.3}$$

Where:

- n_i is intrinsic carrier concentration.
- T is temperature.
- k is the Boltzmann constant.
- τ_{p0} is the excess hole minority carrier lifetime.
- τ_{n0} is the excess electron minority carrier lifetime.
- V_a is the applied voltage.
- D_p and D_n are the diffusion constants of holes and electrons.
- N_d and N_a the electron and hole concentrations.

The diffusion capacitance is dominant under the conditions of forward biased voltage and illumination.

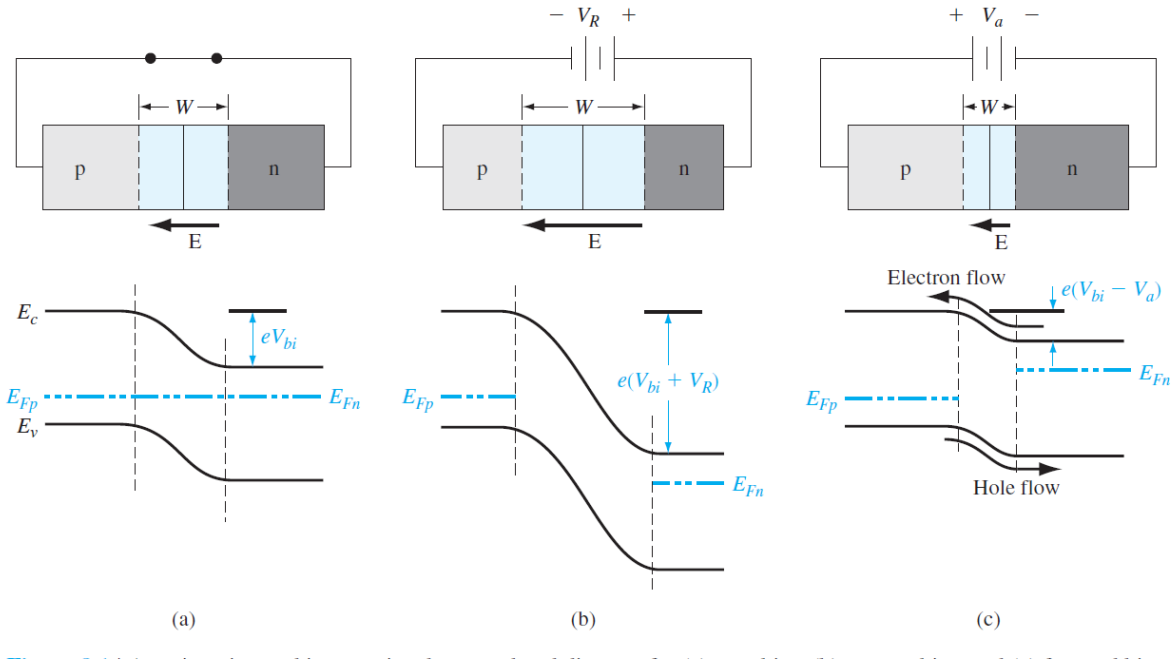

Figure 2.6: Depletion region for different conditions of bias voltage.[20]

According to measurements of the Tektronix company, the capacitance of a silicon solar cell was measured in the dark under reverse biased voltage and the value was close to 0.4µF. In Figure 2.7 the measured capacitance according to the bias voltage is shown.[21]

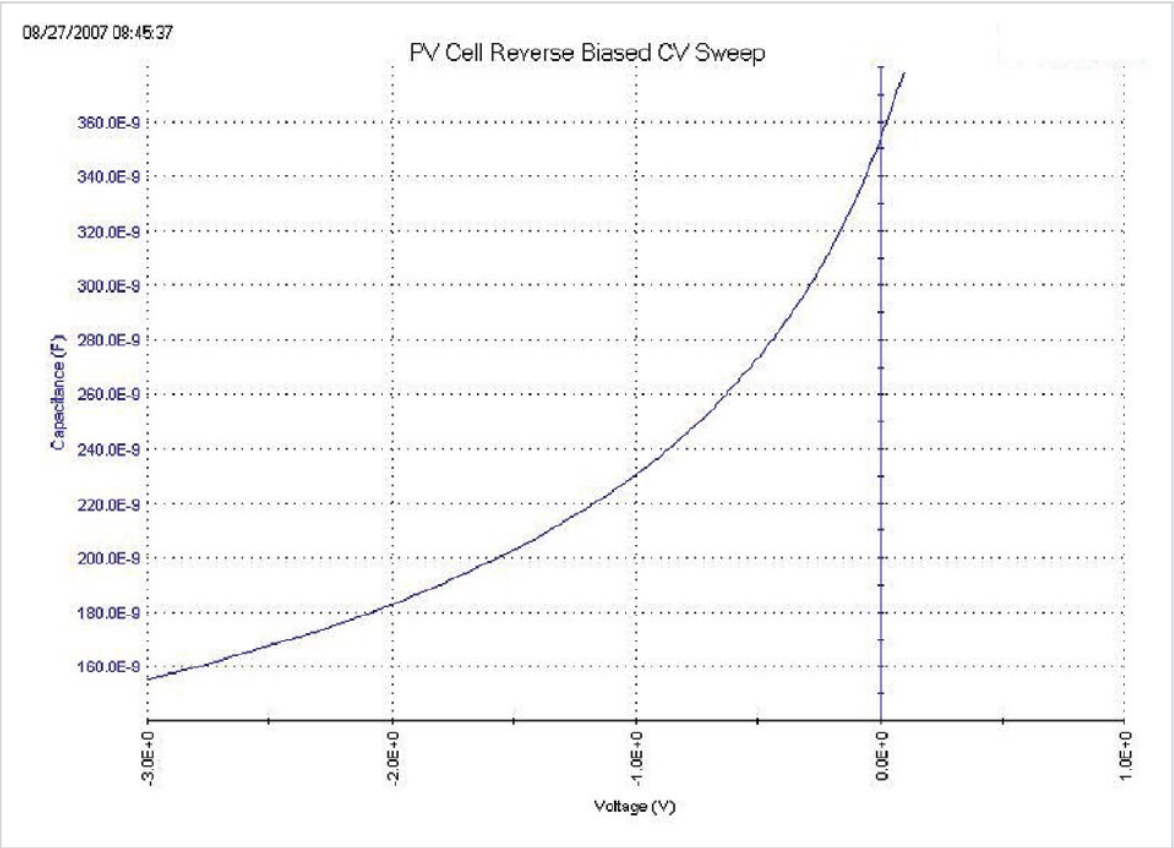

Figure 2.7: Measured capacitance of solar cell for different values of biased voltage.[15]

As it is discussed above, the capacitance increases under forward bias and illumination conditions. In Table 2.1 the results of the simulations of [22] are provided for the capacitance of a silicon solar cell where v is the applied voltage. With a forward biased situation the capacitance can get values of some μF. Also measures from [23] show close results.

TABLE 2.1: Value of capacitance of solar cell based on the applied voltage.

Frequency [kHz]	C [μF]
0,5	0,687·v+2,951
1	0,779·v+2,891
2,5	0,882·v+2,877

In addition to the previous property, the metallization of the solar cell can introduce an inductive behaviour. In the Figure 2.8, a solar cell is shown. The inductance of a conductor is dependent on its dimensions and shape, so the range of values the metallization of the solar cell cannot be very specific. Metallization patterns can lead to different values of inductance. The metallization of the solar cell is the metallic grid that is shown and is consisted of the fingers and the busbars.

The inductance of a typical solar cell metallization pattern is not expected to be very high. However, the metallization can be adapted to increase inductance. Or, an additional metallic layer could be added to add inductance to the solar cell. This must happen on the back of the solar cell since the front metallization is already optimized to minimize shading losses. In an extra project previous to this thesis, simulations with COMSOL Multiphysics have been done with different sizes and geometries of the metallization patterns that fit the dimensions of a 5-inch solar cell. The back metallization of the solar has been adapted so as to achieve higher values of inductance. An example of the simulated geometries is shown in Figure 2.9 where the value of inductance that was calculated from COMSOL Multiphysics was 30 μH. According to the results of the extra project, a maximum value of inductance of about 100 μH is achievable with this approach when a solar cell area equal to 125cm^2 is considered. However, this approach also increases the series resistance of the solar cell. According to the calculations in COMSOL Multiphysics, solar cell series resistance with the additonal metallization can reach the value of 0.45Ω. Based on [24],[25],[26],[27],[28],[29] measurements, the value of a single solar cell series resistance is in the range of 3-10 mΩ.

.

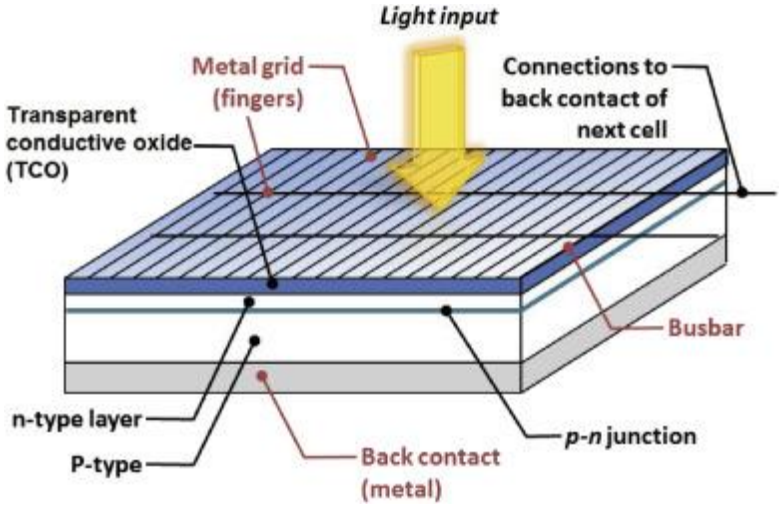

Figure 2.8: Solar cell architecture.[30]

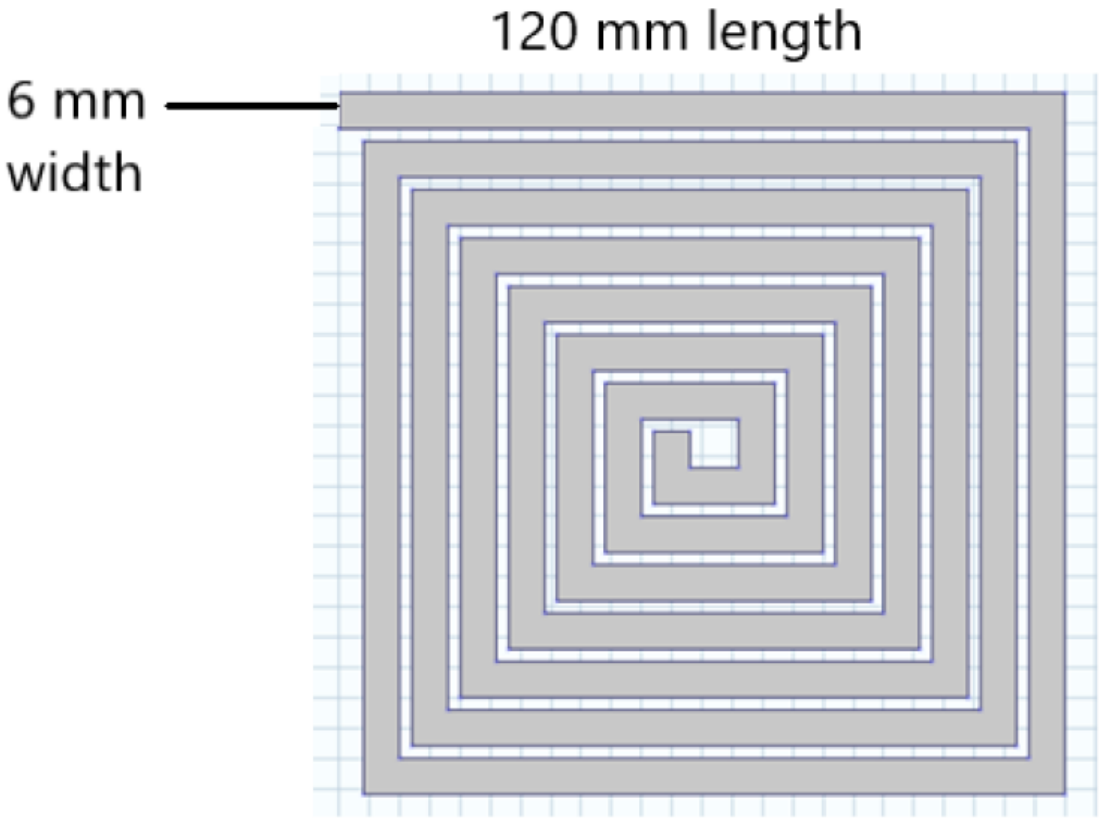

Figure 2.8: Example of solar cell back metallization geometry.

2.2 Model of a solar cell

The behaviour of an ideal solar cell is similar to the behaviour of an ideal diode. The current is described by the equation:

$$I(V) = I_{ph} - I_0\left(e^{\frac{qV}{k_bT}} - 1\right) \tag{2.4}$$

The first term of the right part of equation 2.4 describes the current generated in the solar cell under illumination, also called photogenerated current, whereas the second term describes the dark diode current.

- I_{ph} is the photogenerated current of the cell
- I_0 is the saturation current of the junction
- q is the charge of electron
- k_b is the Boltzmann's constant
- T is the temperature of the solar cell
- V is the biased voltage of the junction

This behaviour can be described with an equivalent circuit made of a current source and a diode, as shown in Figure 2.9. Using an equivalent circuit model is the best way to analyse and simulate the behaviour of the cell.

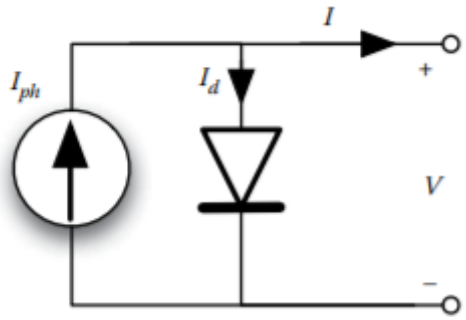

Figure 2.9: Ideal circuit model of solar cell.[31]

The above circuit describes an ideal case where losses and the effect of recombination at the semiconductor are limited. A more realistic solar cell equivalent circuit includes two more components, namely a series and a shunt resistance, as shown in Figure 2.10.

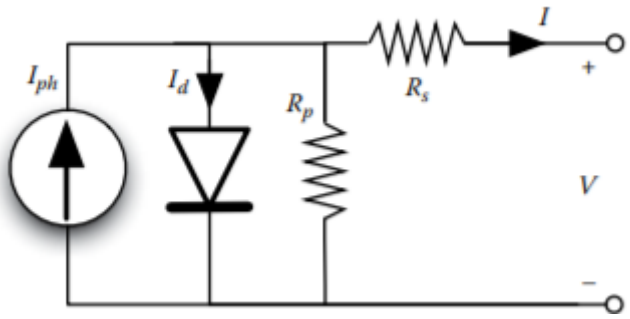

Figure 2.10: Circuit model of solar cell with losses and recombination effect.[31]

Photovoltaic cells are usually characterized – in laboratory – under some specific standard test conditions (STC). These conditions are:

- Irradiance 1000 W/m^2
- AM1.5 spectrum
- Temperature of the solar cell of 25 ^{o}C

Standardization of measurement conditions facilitates comparisons between different photovoltaic devices since, as shown in Figures 2.11 and 2.12, the operation of a solar cell (I-V curve) strongly varies with the temperature of the solar cell and its illumination level. Three parameters must be explained to better understand the I-V curve. Firstly, the short circuit current I_{sc} that is the current that flows out of a solar cell when it is short-circuited. Secondly, the open circuit voltage that is the voltage of the solar cell when there is no circuit connected to it. Thirdly, the maximum power point, that is the operating point at which the solar cell generates the maximum power. In Figures 2.11 and 2.12, T_{max} is the temperature in STC and G_{max} is the irradiance in STC. From the Figures, it is evident that temperature and irradiance affect the operation of the solar cell. From Figure 2.11, it is clear that the increase in the temperature of the cell results in lowering the open circuit voltage. On the other hand, temperature does not affect at all the short circuit current.[7]

From Figure 2.12 the irradiance level has a significant effect in the short circuit current. A decrease in the irradiance lowers the current as well. The open circuit voltage is slightly affected by the irradiance level. STC are very important for the reliable testing and comparison of the solar cells as several conditions affect its operation.

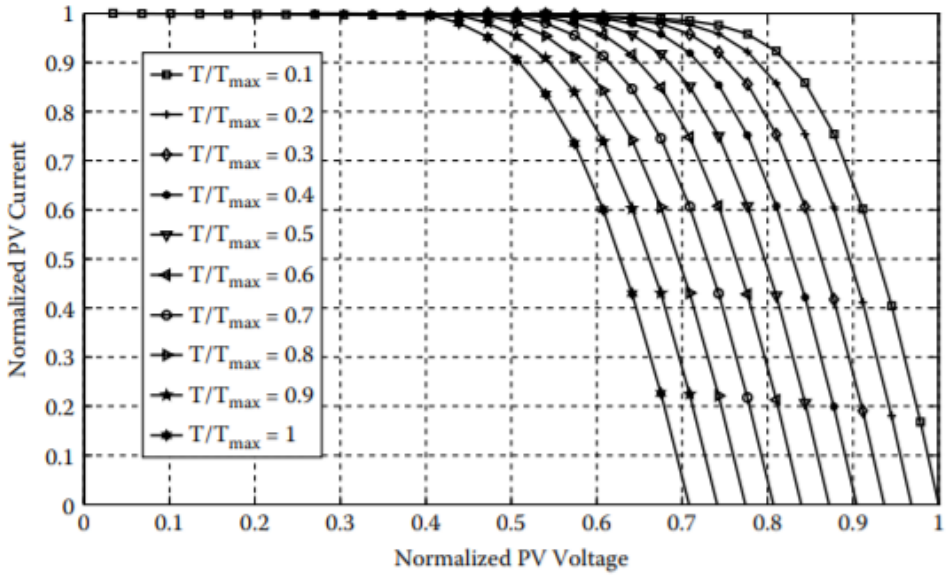

Figure 2.11: Effect of the temperature of the solar cell in the I-V curve.[31]

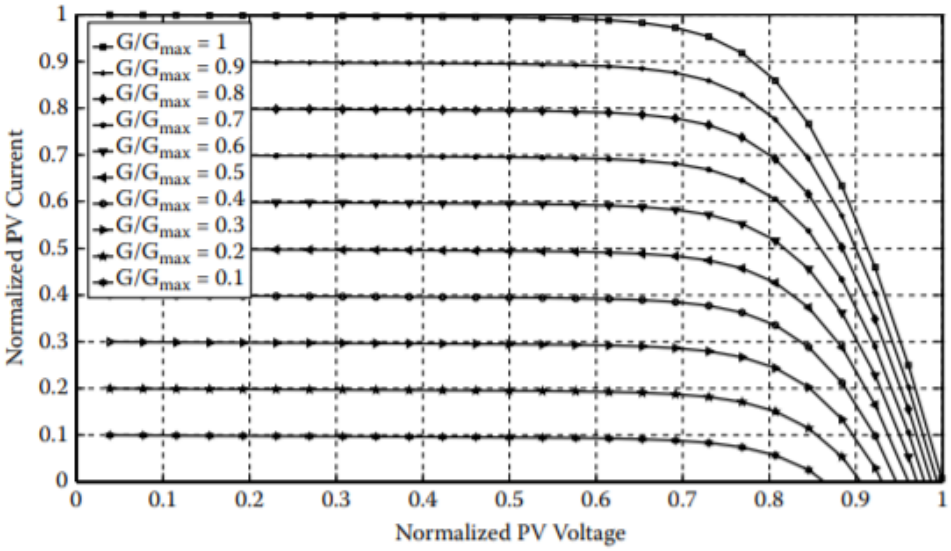

Figure 2.12: Effect of the irradiance on the solar cell in the I-V curve.[31]

Maximum power point trackers (MPPT) are used so that the solar cell always works at the MPP. In Figure 2.13 the effect of different illumination levels on the MPP is shown.

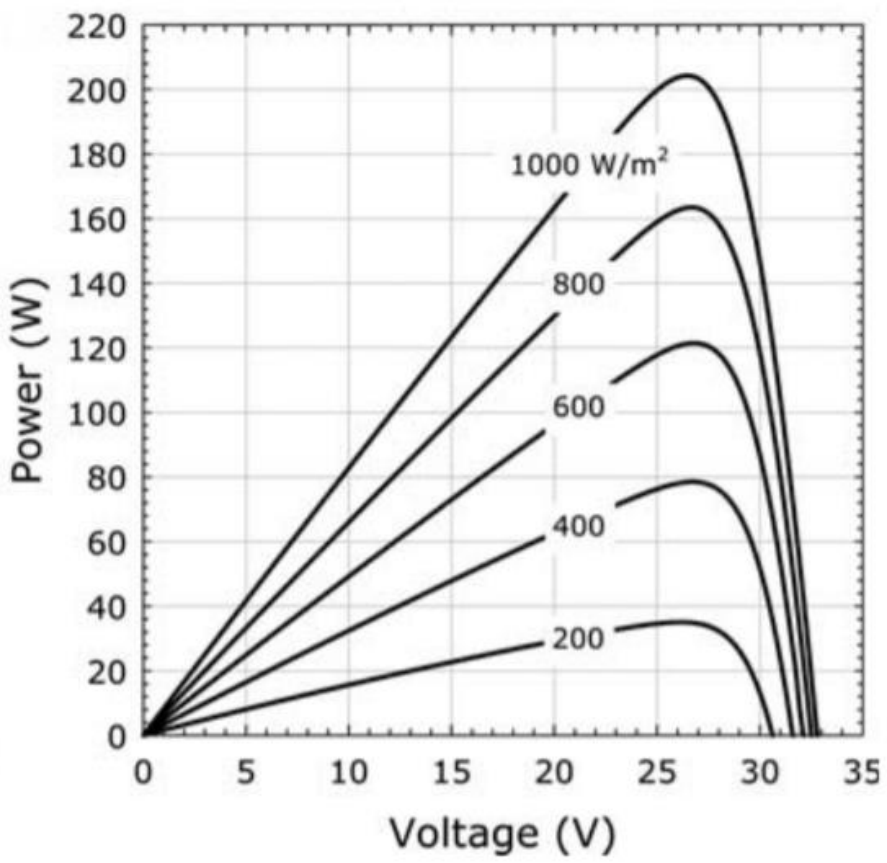

Figure 2.13: P-V curve for different illumination levels.[32]

Based on the analysis above, the circuit model that describes the solar cell in a more realistic point of view is displayed in Figure 2.14. In this circuit the inductive and capacitive behaviour of the solar cell are taken into consideration and this is a complete model.

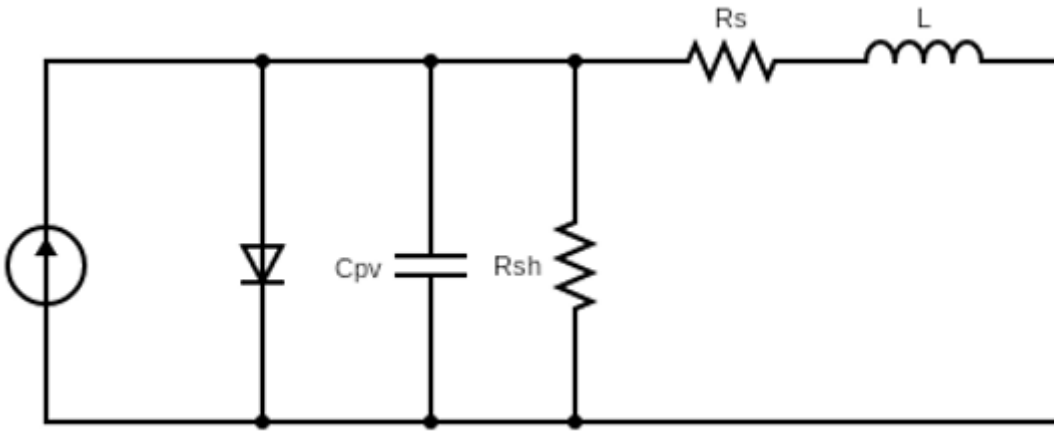

Figure 2.14: Equivalent circuit model of solar cell with inductance and capacitance.

Chapter 3: State space averaging and ripple analysis for the proposed system

3.1 Inductorless power conversion in solar cells

In order to benefit from the photovoltaic effect and get the power from the solar cell, power converters are used. Converters use capacitors and inductors to work, but as it is already stated in Chapter 2, a solar cell has already a capacitive and an inductive behaviour. A typical circuit with a boost converter and a solar panel is shown in Figure 3.1.

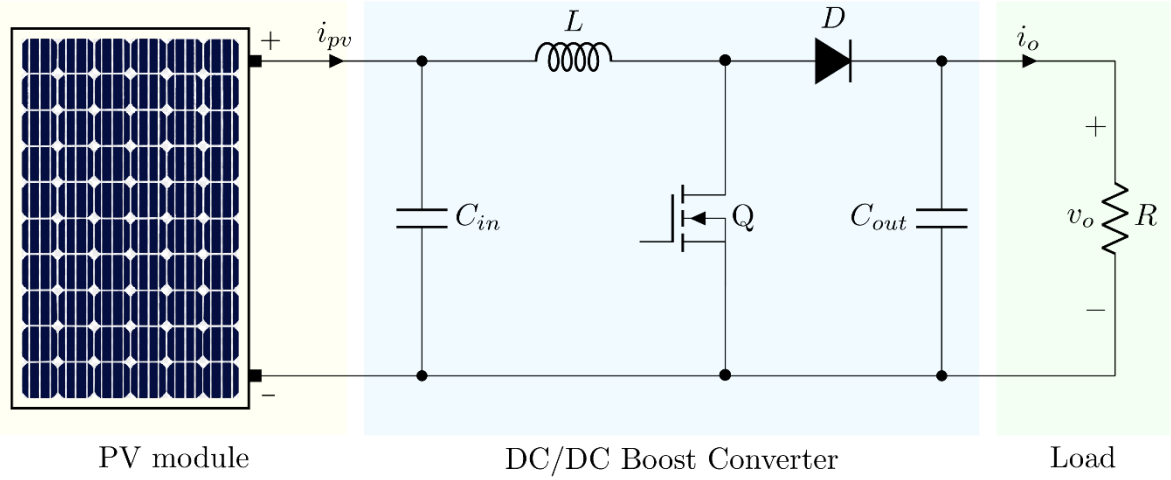

Figure 3.1: Boost converter with PV module.[33]

Inductors that are used in converters are huge in comparison with other components of the system and have many losses. The size of the inductors makes it difficult to implement converters in several applications. Of course, there are inductors that are made with smaller dimensions, but the cost is higher. The bigger the size of the inductor the higher the losses that it has. [34]

Another factor that is important is that the inductor cores can have severe losses. With the properties that were referred above for the equivalent circuit of a solar cell, a PV module with a boost converter circuit can be as shown in Figure 3.2.

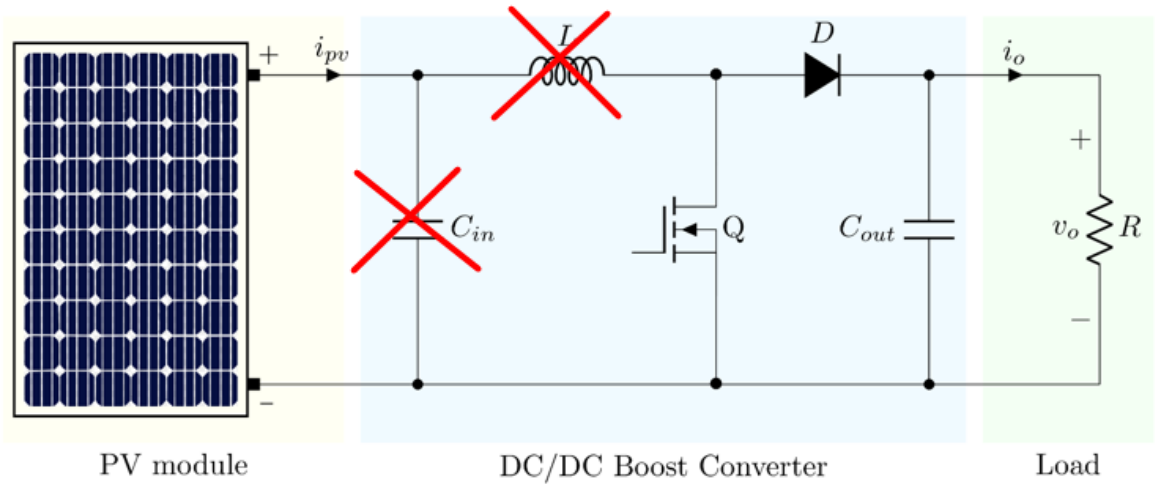

Figure 3.2: Model of a PV module and a boost converter with the inductive and capacitive behaviour of the module.

The capacitance and the inductance can be provided from the solar cell and this can lead to two basic advantages:

- Elimination of inductor core losses
- Easier implementation of the power converter due to smaller size

3.2 Linearization of the system

The incident illumination on a solar cell is changing very often. There are many factors that change the level of the illumination such as the position of the sun or the atmospheric condition (clear sky or cloudy weather). This means that the state of the system is changing abruptly during operation. As it is discussed in the previous chapter, a change in irradiance or temperature changes the I-V curve of the photovoltaic cell. This means that the optimal operating point, that is the point at which the cell generate the maximum power, also called Maximum Power Point (MPP) also changes. In Figure 3.3 there is an example of the MPP on the I-V curve.

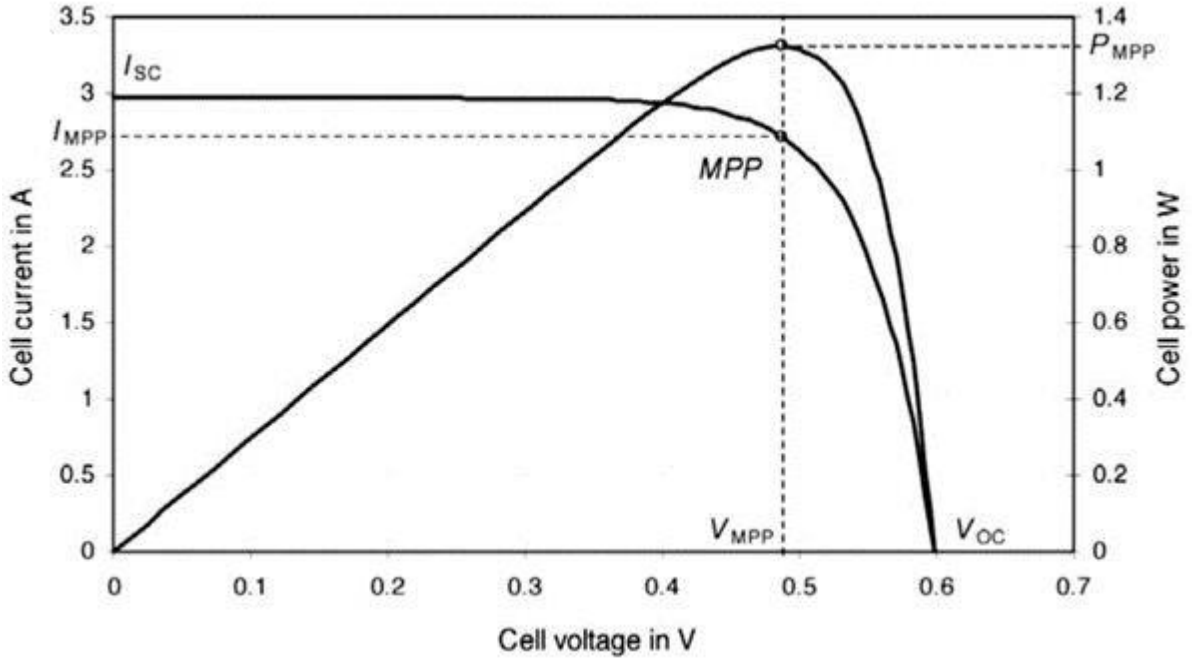

Figure 3.3: I-V and P-V curve of a solar cell.[35]

Since MPP changes during operation, it must be continuously tracked. This process is called maximum power point tracking (MPPT). There are several methods to track the MPP and can be categorized as follows:

- Indirect MPPT, the MPP is estimated through models.
- Direct MPPT, the MPP is defined through the I-V curve.

One example of indirect MPPT is the fractional open circuit voltage method. In this method the V_{mpp} is given by:

$$V_{mmp} = k\ x\ V_{oc} \tag{3.1}$$

Where k is a constant value and is dependent on the solar cell technology. V_{oc} can be easily tracked and thus, by multiplying with the constant k, the MPP can be calculated. The basic drawback of this method is that the exact MPP is not easily achieved since the constant k is an estimation and the solar cell operating point is close to the MPP. Also, during the time in which V_{oc} is measured, no power is produced by the solar cell.[5], [36]

An example of a direct MPPT is the Perturb and observe (P&O) method, which is the most popular direct technique. The working principle of P&O method is the following:

1. The solar cell voltage is perturbed.
2. The perturbation leads to a change in power.
3. If an increase (decrease) in the voltage leads to an increase in power, the MPP is at higher (lower) voltage.

4. If an increase (decrease) in the voltage leads to a decrease in power, the MPP is at lower (higher) voltage.

In Table 3.1 the algorithm that describes the P&O method is shown. As it is explained above through voltage perturbations the MPP is tracked.

TABLE 3.1: Algorithm of P&O method.[37]

Perturbation	Change in Power	Next Perturbation
Positive	Positive	Positive
Positive	Negative	Negative
Negative	Positive	Negative
Negative	Negative	Positive

The flowchart of P&O method is shown in Figure 3.4, where T_p is the time interval between each perturbation. It is very important to determine the value of T_p as short time can confuse the MPPT and the operating point will be unstable. If T_p has a high value, it can penalize the MPPT speed.[31]

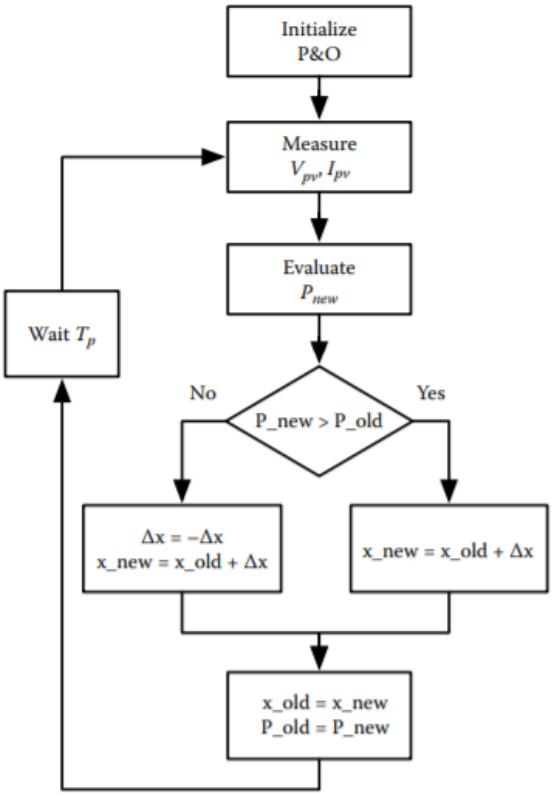

Figure 3.4: Flowchart of P&O method.[31]

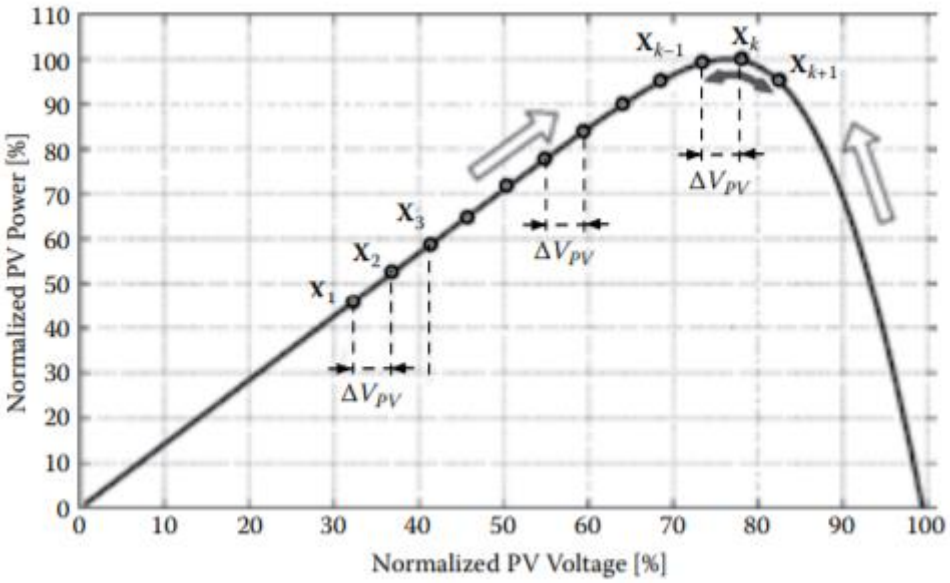

Figure 3.5: PV cell operating point imposed by P&O method.[31]

The continuing change of MPP, as shown in Figure 3.5, adds a dynamic behaviour to the system. The equation that describes the change in voltage with the P&O method is:

$$x_{((k+1)T_p)} = x_{kT_p} \pm \quad x = x_{kT_p} \pm (x_{kT_p} - x_{\left((k-1)T_p\right)})sign(P_{(kT_p)} - P_{((k-1)T_p)}) \quad (3.2)$$

The *x* variable in equation 3.2 represents the perturbation, for example the change in the duty cycle.

This equation is a non-linear equation and should be analysed with specific models in order to linearize it. A time domain analysis in both steady-state and dynamic situation allows an optimization of the values of P&O. The analysis should be done with the small signal model around the operating point of the solar cell, ideally the MPP. The system oscillates around MPP as the P&O method continuously tracks it. The linearization of any variable $y(t)$ of a system can be done by defining its DC value Y and its small-signal variation $\tilde{y}(t)$:

$$y(t) = Y + \tilde{y}(t)$$

An example of such a linearization for a diode is now shown. This could be applied for instance to the PV cell diode (see Figure 2.14). The voltage of the diode can be linearized as follows:

$$v_{in}(t) = V_{in} + \tilde{v}_{in}(t) \quad (3.3)$$

Where:

- V_{in} is the DC operating voltage of the diode
- $\tilde{v}_{in}(t)$ is the AC small signal variation

The current of a diode can be described by the equation 3.4:

$$i_d(t) = I_0\left(e^{\frac{v_{in}(t)}{nV_T}} - 1\right) = I_d + \tilde{\imath}_d(t) \tag{3.4}$$

Where:

- I_d is the DC operating current of the diode
- $\tilde{\imath}_d(t)$ is the AC small signal variation

Taylor series expansion can be used to linearize equation 3.4 around the operating point (V_{in}). The equation of Taylor series is:

$$f(x) = \sum_{n=0}^{\infty} \frac{1}{n!} \frac{d^n f(x)}{dx^n}|_{x=x_0}(x - x_0)^n \; = f(x_0) + \frac{df(x)}{dx}|_{x=x_0}(x - x_0)^n \tag{3.5}$$

Thus, the function of the current Taylor series is:

$$\begin{aligned} i_d\big(v_{in}(t)\big) &= I_0\left(e^{\frac{V_{in}}{nV_T}} - 1\right) + \frac{di_d(V_{in})}{dv_{in}}|_{v_{in}=V_{in}}(v_{in} - V_{in}) \\ &= I_0\left(e^{\frac{V_{in}}{nV_T}} - 1\right) + \frac{I_0}{nV_T}e^{\frac{v_{in}(t)}{nV_T}}\,|_{v_{in}=V_{in}}(v_{in} - V_{in}) \\ &= I_0\left(e^{\frac{V_{in}}{nV_T}} - 1\right) + \frac{I_0}{nV_T}e^{\frac{V_{in}}{nV_T}}\,\tilde{v}_{in}(t) \\ &= I_d(V_{in}) + \frac{\tilde{v}_{in}(t)}{\frac{nV_T}{I_0}e^{-\frac{V_{in}}{nV_T}}} \end{aligned} \tag{3.6}$$

Where:

- $I_d(V_{in})$ is the DC operating current of the diode
- $\frac{\tilde{v}_{in}(t)}{\frac{nV_T}{I_0}e^{-\frac{V_{in}}{nV_T}}}$ is the AC small signal variation

By defining the dynamic resistance of the diode as $r_d = \frac{nV_T}{I_0}e^{-\frac{V_{in}}{nV_T}}$, the equation becomes:

$$i_d\big(v_{in}(t)\big) = I_d(V_{in}) + \frac{\tilde{v}_{in}(t)}{r_d} \tag{3.7}$$

3.3 State space averaging and ripple analysis

In order to model the realistic performance of an electric circuit DC analysis, small signal AC and ripple analysis should be analysed. In Figure 3.6 such a behaviour is shown for an electric circuit. In this Figure, a steady state for a system is changing and an AC behaviour occurs. The system faces an overshoot in the value of current until it reaches a new steady state. Ripple exists in the whole operation of the system.

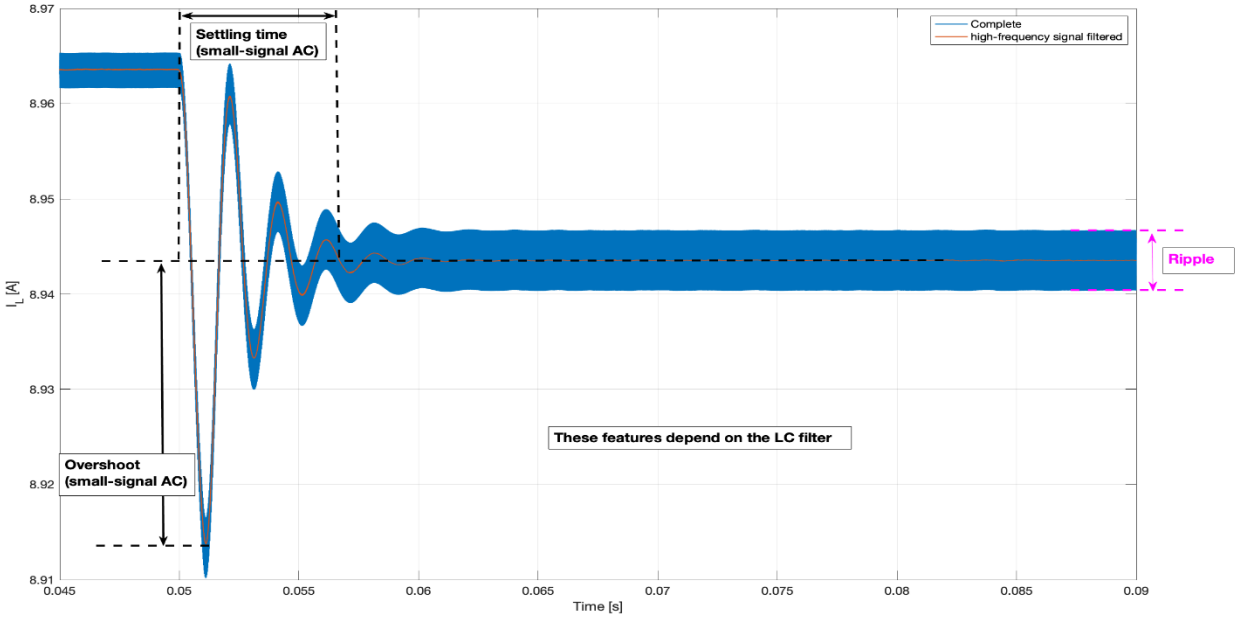

Figure 3.6: DC, AC and ripple in an electric circuit.

State space averaging

State space averaging method is a technique to model AC converters. State space averaging uses the description of state space of system so as to derive the small signal averaged equations of the converter. It can provide both DC and AC solutions for a system. State space averaging is the state of equations that describes the equilibrium and small signal AC models. The equations are dependent on the circuit equations of each sub-interval (switch on and off). To create these equations first the state vector **x**(t), the input vector **u**(t) and the output vector **y**(t) have to be defined. The assumption that has to be done so that this model is close to the real performance of the circuit is that the natural frequency of the converter and the frequencies of the variations of the converter inputs are slower than the switching frequency [38]. Duty cycle is important to introduced and is the ration between the turn on time and turn off time of the converter.

The circuit below in Figure 3.7 is the circuit of the system based on the models that were discussed in the previous Chapters.

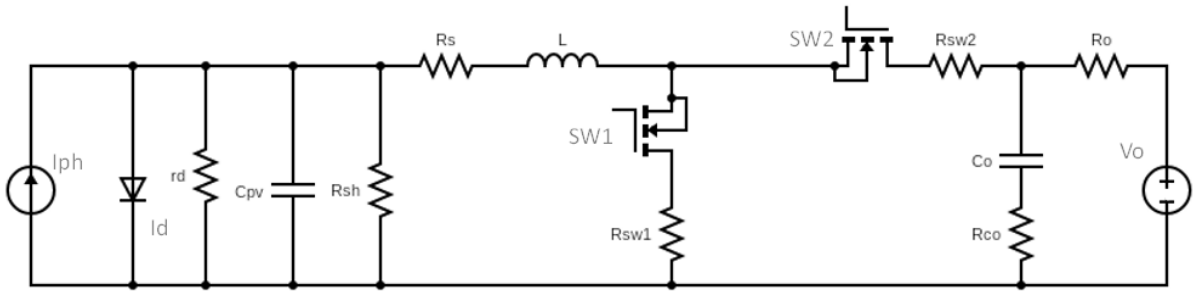

Figure 3.7: Equivalent circuit of the system.

Where:

- I_{ph} is the photocurrent
- I_d is based on the model of state space averaging
- r_d is the dynamic resistance of the system
- C_{pv} is the capacitance of the solar cell
- R_{sh} is the shunt resistance of the solar cell
- R_s is the series resistance of the solar cell
- L is the inductance of the solar cell
- R_{sw1} is the resistance of SW1
- R_{sw2} is the resistance of SW2
- C_o is the output capacitor of the converter
- R_{co} is the resistance of the output capacitor
- R_o is the load resistance
- V_o is the output voltage

The t_{on} is the time interval when the first switch is closed and the second is open, as shown in Figure 3.8, and t_{off} time interval is when the first switch is open and the second is closed, as shown in Figure 3.9.

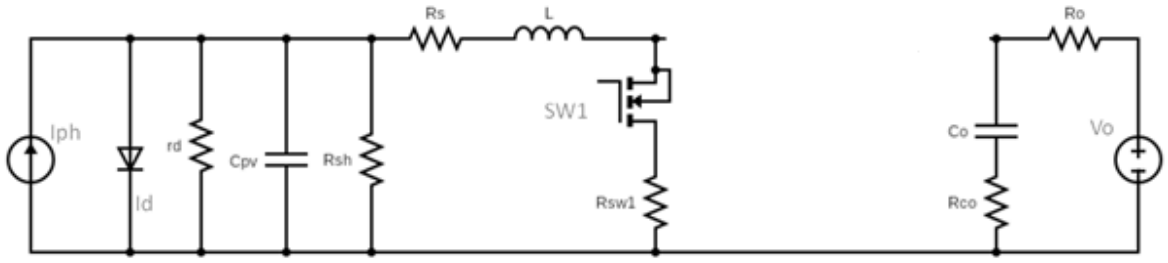

Figure 3.8: Circuit during $t_{on.}$

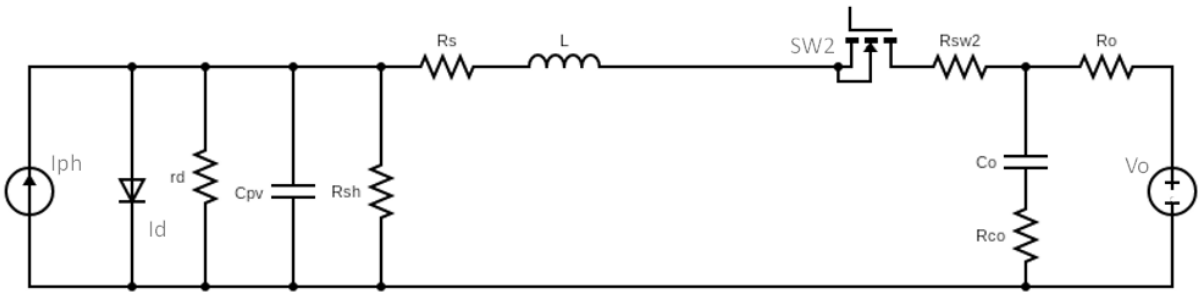

Figure 3.9: Circuit during $t_{off.}$

Considering the system in Figure 3.7 the state, input and output vectors are:

$$x(t) = \begin{bmatrix} i_L(t) \\ V_{in}(t) \\ V_{co}(t) \end{bmatrix}, u(t) = \begin{bmatrix} I_{ph} \\ I_D \\ V_o \end{bmatrix}, \ y(t) = [i_o(t)] \tag{3.8}$$

The next equations provide the small-signal AC model [38]:

$$K\frac{d\hat{x}(t)}{dt} = A\hat{x}(t) + B\hat{u}(t) + \{(A_1 - A_2)X + (B_1 - B_2)U\}\hat{d}(t)$$

$$\hat{y}(t) = C\hat{x}(t) + E\hat{u}(t) + \{(C_1 - C_2)X + (E_1 - E_2)U\}\hat{d}(t) \tag{3.9}$$

Where:

$$A = DA_1 + D'A_2$$

$$B = DB_1 + D'B_2$$

$$C = DC_1 + D'C_2$$

$$E = DE_1 + D'E_2$$

With D being the duty cycle of the converter

And:

$$0 = AX + BU$$

$$Y = CX + EU$$

The first step is to build the equations for each subinterval (t_{on} and t_{off}) , and these equations are given from:

For t_{on}:

$$K\frac{dx(t)}{dt} = A_1x(t) + B_1u(t)$$
$$y(t) = C_1x(t) + E_1u(t) \quad (3.10)$$

Becomes:

$$\begin{bmatrix} L & 0 & 0 \\ 0 & C_{pv} & 0 \\ 0 & 0 & C_o \end{bmatrix}\frac{d}{dt}\begin{bmatrix} i_L(t) \\ V_{in}(t) \\ V_{co}(t) \end{bmatrix} = \begin{bmatrix} -(R_s + R_{sw1}) & 1 & 0 \\ -1 & \frac{-1}{r_d//R_{sh}} & 0 \\ 0 & 0 & \frac{-1}{R_o + R_{co}} \end{bmatrix}\begin{bmatrix} i_L(t) \\ V_{in}(t) \\ V_{co}(t) \end{bmatrix} +$$

$$\begin{bmatrix} 0 & 0 & 0 & 0 \\ 1 & -1 & 0 & 0 \\ 0 & 0 & \frac{+1}{R_o+R_{co}} & 0 \end{bmatrix}\begin{bmatrix} I_{ph} \\ I_D \\ V_o \end{bmatrix} \quad (3.11)$$

$$[i_o(t)] = \begin{bmatrix} 0 & 0 & \frac{1}{R_o+R_{co}} \end{bmatrix}\begin{bmatrix} i_L(t) \\ V_{in}(t) \\ V_{co}(t) \end{bmatrix} + \begin{bmatrix} 0 \\ 0 \\ \frac{-1}{R_o+R_{co}} \\ 0 \end{bmatrix}\begin{bmatrix} I_{ph} \\ I_D \\ V_o \end{bmatrix} \quad (3.12)$$

For t_{off}:

$$K\frac{dx(t)}{dt} = A_2x(t) + B_2u(t)$$
$$y(t) = C_2x(t) + E_2u(t) \quad (3.13)$$

Becomes:

$$\begin{bmatrix} L & 0 & 0 \\ 0 & C_{pv} & 0 \\ 0 & 0 & C_o \end{bmatrix} \frac{d}{dt} \begin{bmatrix} i_L(t) \\ V_{in}(t) \\ V_{co}(t) \end{bmatrix} = \begin{bmatrix} -\left(R_s + R_{sw2} + \frac{R_o R_{co}}{R_o + R_{co}}\right) & 1 & -\frac{R_o}{R_o + R_{co}} \\ -1 & \frac{-1}{r_d // R_{sh}} & 0 \\ \frac{R_o}{R_o + R_{co}} & 0 & \frac{1}{R_o + R_{co}} \end{bmatrix} \begin{bmatrix} i_L(t) \\ V_{in}(t) \\ V_{co}(t) \end{bmatrix} +$$

$$\begin{bmatrix} 0 & 0 & \frac{-R_{co}}{R_o + R_{co}} & -1 \\ 1 & -1 & 0 & 0 \\ 0 & 0 & \frac{-1}{R_o + R_{co}} & 0 \end{bmatrix} \begin{bmatrix} I_{ph} \\ I_D \\ V_o \end{bmatrix} \tag{3.14}$$

$$[i_o(t)] = \begin{bmatrix} \frac{R_o}{R_o + R_{co}} & 0 & \frac{1}{R_o + R_{co}} \end{bmatrix} \begin{bmatrix} i_L(t) \\ V_{in}(t) \\ V_{co}(t) \end{bmatrix} + \begin{bmatrix} 0 \\ 0 \\ \frac{-1}{R_o + R_{co}} \\ 0 \end{bmatrix} \begin{bmatrix} I_{ph} \\ I_D \\ V_o \end{bmatrix} \tag{3.15}$$

By substituting the matrices in the AC small-signal equations the model is ready. The differential equations are solved with the use of MATLAB.

Ripple analysis

For the ripple analysis, Kirchhoff's laws should be applied, as shown in Figure 3.7, for the two subintervals. The analysis is as follows:

For t_{on}:

$$C_{pv} \frac{dV_{in}(t)}{dt} = I_{ph} - I_D - \frac{V_{in}(t)}{r_d // R_{sh}} - i_L(t) \tag{3.16}$$

$$L \frac{di_L(t)}{dt} = V_{in}(t) - (R_s + R_{sw1}) i_L(t) \tag{3.17}$$

$$C_o \frac{dV_{co}}{dt} = \frac{V_o - V_{co}(t)}{R_o + R_{co}} \tag{3.18}$$

$$i_o(t) = \frac{V_{co}(t) - V_o}{R_o + R_{co}} \tag{3.19}$$

For t_{off}:

$$C_{pv} \frac{dV_{in}(t)}{dt} = I_{ph} - I_D - \frac{V_{in}(t)}{r_d // R_{sh}} - i_L(t) \tag{3.20}$$

$$L \frac{di_L(t)}{dt} = V_{in}(t) - (R_s + R_{sw2}) i_L(t) - i_o(t) R_o - V_o \tag{3.21}$$

$$C_o \frac{dV_{co}}{dt} = i_L(t) \frac{R_o}{R_o + R_{co}} + \frac{V_o - V_{co}}{R_o + R_{co}} \tag{3.22}$$

$$i_o(t) = i_L(t)\frac{R_{co}}{R_o+R_{co}} + \frac{V_{co}-V_o}{R_o+R_{co}} \tag{3.23}$$

So, the second equation for t_{off} can be written as:

$$L\frac{di_L(t)}{dt} = V_{in}(t) - \left(R_s + R_{sw2} + \frac{R_o R_{co}}{R_o+R_{co}}\right) i_L(t) - V_o - \frac{V_{co}-V_o}{R_o+R_{co}} R_o \tag{3.24}$$

For the ripple analysis the equations for t_{on} and t_{off} have to be solved.

For t_{on}:

$$C_{pv}\frac{dV_{in}(t)}{dt} = I_{ph} - I_D - \frac{V_{in}(t)}{r_d//R_{sh}} - i_L(t) \tag{3.25}$$

$$L\frac{di_L(t)}{dt} = V_{in}(t) - (R_s + R_{sw1})i_L(t) \tag{3.26}$$

This pair of differential equations is a linear non-homogenous system in the following form:

$$y_1' = a_{11}y_1 + a_{12}y_2 + b_1 \tag{3.27}$$

$$y_2' = a_{21}y_1 + a_{22}y_2 + b_2 \tag{3.28}$$

In order to solve the system, first we differentiate the first equation and substitute y_2', so we get the form:

$$y_1'' + fy_1' + gy_1 = h \tag{3.29}$$

Where:

$$f = -a_{11} - \frac{a'_{12}}{a_{12}} - a_{22}$$

$$g = a'_{11} + \frac{a'_{12}a_{11}}{a_{12}} - a_{12}a_{21} + a_{22}a_{11}$$

$$h = -\left(\frac{a'_{12}}{a_{12}} + a_{22}\right) b_1 + a_{12}b_2 + b_1' \tag{3.30}$$

For the first subinterval the parameters take the values that are shown below.

$$y_1' = \frac{dV_{in}(t)}{dt}, \quad y_2' = \frac{di_l(t)}{dt}$$

$$a_{11} = \frac{-1}{r_d//R_{sh}C_{pv}}, \quad a_{12} = \frac{-1}{C_{pv}}$$

$$y_1 = V_{in}(t), \quad y_2 = i_L(t)$$

$$a_{21} = \frac{1}{L}, \quad a_{22} = -\frac{R_s+R_{sw1}}{L}, \quad b_1 = \frac{I_{ph}-I_D}{C_{pv}}, \quad b_2 = 0 \tag{3.31}$$

After substituting all the parameters, the result is:

$$\frac{d^2V_{in}(t)}{dt^2} - \left(\frac{-1}{r_d//R_{sh}C_{pv}} - \frac{R_s+R_{sw1}}{L}\right)\frac{dV_{in}(t)}{dt} + \left(\frac{R_s+R_{sw1}}{Lr_d//R_{sh}C_{pv}} + \frac{1}{LC_{pv}}\right)V_{in} = \left(\frac{I_{ph}-I_D}{C_{pv}}\right)\left(\frac{R_s+R_{sw1}}{L}\right) \tag{3.32}$$

$$a = -\left(\frac{-1}{r_d//R_{sh}C_{pv}} - \frac{R_s+R_{sw1}}{L}\right)$$

$$b = \left(\frac{R_s+R_{sw1}}{Lr_d//R_{sh}C_{pv}} + \frac{1}{LC_{pv}}\right)$$

$$c = \left(\frac{I_{ph}-I_D}{C_{pv}}\right)\left(\frac{R_s+R_{sw1}}{L}\right) \tag{3.32}$$

This equation is a linear nonhomogeneous second order differential equation. The solution of this equation is the sum of the solution of the homogeneous and another partial solution of this equation.

The solution of the homogeneous is shown:

$$\frac{d^2V_{in}(t)}{dt^2} - \left(\frac{-1}{r_d//R_{sh}C_{pv}} - \frac{R_s+R_{sw1}}{L}\right)\frac{dV_{in}(t)}{dt} + \left(\frac{R_s+R_{sw1}}{Lr_d//R_{sh}C_{pv}} + \frac{1}{LC_{pv}}\right)V_{in} = 0 \tag{3.33}$$

The solution of the homogeneous is given by function

$$y_1 = e^{rt}$$

$$y_1' = re^{rt} \tag{3.34}$$

$$y_1'' = r^2e^{rt}$$

So, the form of the solution of the homogenous equation is

$$e^{rt}(r^2 + ar + b) = 0 \tag{3.35}$$

$$(r^2 + ar + b) = 0 => \Delta = a^2 - 4b$$

If Δ>0 then the solutions of the polynomial are:

$$r_{1,2} = \frac{-a \pm \sqrt{a^2-4b}}{2} \tag{3.36}$$

and it means that the system is overdamped.

If the Δ=0 the solution of the polynomial is a double root and is:

$$r_{1,2} = \frac{-a}{2} \tag{3.37}$$

and it means that the system is critically damped.

If Δ<0 the solutions of the polynomial are:

$$r_{1,2} = \frac{-a \pm i\ \sqrt{a^2-4b}}{2} \tag{3.38}$$

and it means that the system is underdamped. A deeper analysis for the damping cases is done in the next part of small signal model.

Then, in order to solve the nonhomogeneous another partial solution one solution must be added to the solution of the homogeneous. This solution can be

$$y_1 = c/b \tag{3.39}$$

If it is put at the differential equation of the input voltage it can be easily seen that is a partial solution.

The complete solution of the system by following this methodology is:

$$V_{in}(t) = C_1 e^{rt} + C_2 e^{-rt} + \frac{c}{b} \tag{3.40}$$

The current of the inductor can be found by substituting the input voltage to the following equation:

$$i_L(t) = I_{ph} - I_D - \frac{V_{in}(t)}{r_d//R_{sh}} - C_{pv}\frac{dV_{in}(t)}{dt} \tag{3.41}$$

After some algebra the current is:

$$i_L(t) = I_{ph} - I_D - \frac{r_d+R_{sh}}{r_d R_{sh}}(C_1 e^{rt} + C_2 e^{-rt} + \frac{c}{b}) - C_{pv}(C_1 r e^{rt} - C_2 r e^{-rt}) \tag{3.42}$$

For the voltage at the output capacitor the differential equation is:

$$C_o\frac{dV_{co}}{dt} = \frac{V_o - V_{co}(t)}{R_o + R_{co}} => \frac{dV_{co}}{V_o - V_{co}(t)} = \frac{C_o dt}{R_o + R_{co}} =>$$

$$\ln(V_o - V_{co}) = -\frac{C_o t}{R_o+R_{co}} + C_3 => V_{co}(t) = V_o - e^{-\frac{C_o t}{R_o+R_{co}}+C_3} \tag{3.43}$$

For the second subinterval the same methodology is followed. The equations are given above for t_{off}. In this subinterval the situation is more complex as all three differential equations are connected to each other. In order to solve this linear system of the three differential

equations, the first equation has to be differentiated two times. After some algebra the result is:

$$C_{pv}\frac{d^3Vin}{dt^3} = -\frac{d^2Vin}{dt^2}\frac{r_d+R_{sh}}{r_dR_{sh}} - \frac{d^2i_L}{dt^2} \tag{3.44}$$

$$L\frac{d^2i_L}{dt^2} = \frac{dV_{in}}{dt} - \left(R_s + R_d + \frac{R_oR_{co}}{R_o+R_{co}}\right)\frac{di_L}{dt} - \frac{dV_{co}}{dt}\frac{R_o}{R_{co}+R_o} \tag{3.45}$$

$$C_o\frac{dV_{co}}{dt} = i_L(t)\frac{R_o}{R_o+R_{co}} + \frac{V_o-V_{co}}{R_o+R_{co}} \tag{3.46}$$

Where

$$\frac{V_{co}-V_o}{R_o+R_{co}} = \frac{V_{in}(t)-\left(R_s+R_d+\frac{R_oR_{co}}{R_o+R_{co}}\right)i_L(t)-V_o-V_d-L\frac{di_L(t)}{dt}}{R_o} \tag{3.47}$$

and

$$i_L(t) = I_{ph} - I_D - \frac{V_{in}(t)(r_d+R_o)}{r_dR_{sh}} - C_{pv}\frac{dV_{in}(t)}{dt} \tag{3.48}$$

After substituting all the equations at the first, the result is a 3rd order non-homogeneous linear equation in the following form:

$$\frac{d^3Vin}{dt^3} + g\frac{d^2Vin}{dt^2} + h\frac{dV_{in}}{dt} + kV_{in} = l \tag{3.49}$$

With

$$g = \frac{V_d + V_o - (I_d - I_{ph})\left(R_d + R_s + \frac{(R_{co}R_o)}{(R_{co} + R_o)}\right) + \frac{R_o^2(I_d - I_{ph})}{C_oL(R_{co}R_o)^2}}{C_oC_{pv}L(R_{co}+R_o)}$$

$$h = -\frac{\left((R_{sh}+r_d)\left(R_d+R_s+\frac{R_{co}R_o}{R_{co}+R_o}\right)\right)}{R_{sh}r_d} - \frac{R_o^2(R_{sh}+r_d)}{(C_oLR_{sh}r_d(R_{co}+R_o)^2)} + 1}{(C_oC_{pv}L(R_{co}+R_o))}$$

$$k = \frac{\left(\frac{1}{L} - C_{pv}\left(R_d+R_s+\frac{R_{co}R_o}{Rco+Ro}\right) - \frac{L(R_{sh}+r_d)}{R_{sh}r_d} + \frac{(R_{sh}+r_d)\left(R_d+R_s+\frac{R_{co}R_o}{R_{co}+R_o}\right)}{R_{sh}r_d} + \frac{C_{pv}R_o^2}{C_oL(R_{co}+R_o)^2}\right)}{C_oC_{pv}L(R_{co}+R_o)}$$

$$l = \frac{C_{pv}L - C_{pv}\left(R_d + R_s\frac{R_{co}R_o}{R_{co}+R_o}\right) + \frac{R_{sh}+r_d}{R_{sh}r_d}}{C_oC_{pv}L(R_{co}+R_o)}$$

Same as at the 1st subinterval, the solution of the homogeneous is given by the function

$$\begin{aligned} y_1 &= e^{rt} \\ y_1' &= re^{rt} \\ y_1'' &= r^2e^{rt} \\ y_1''' &= r^3e^{rt} \end{aligned} \tag{3.50}$$

So, the form of the solution of the homogenous is

$$e^{rt}(r^3 + gr^2 + hr + k) = 0 \tag{3.51}$$

It is a 3rd order polynomial, and it has 3 roots. So, in this case the input voltage is

$$V_{in}(t) = C_4e^{r_1t} + C_5e^{r_2t} + C_6e^{r_3t} + \frac{l}{k} \tag{3.51}$$

Where $\frac{l}{k}$ is the partial solution of the nonhomogeneous equation for the input voltage.

By substituting the input voltage into the other equations and by doing some algebra the current of the inductor and the voltage of the output capacitor are:

$$i_L(t) = I_{ph} - I_D - \frac{r_d+R_{sh}}{r_dR_{sh}}(C_4e^{r_1t} + C_5e^{r_2t} + C_6e^{r_3t} + \frac{l}{k}) - C_{pv}(C_4r_1e^{r_1t} + C_5r_2e^{r_2t} + C_6r_3e^{r_3t}) \tag{3.52}$$

Also ripple equations are set in MATLAB as the ones for the state space averaging.

3.4 Calculation of losses

Losses in DC-DC converter can be divided into two parts, conduction losses and switching losses. Conduction losses are dependent on the resistive part of the circuit as these losses are major. In addition to this, switching losses of the switch occur when the switch changes its

situation (from open to close and vice versa) and have some impact on the general losses of the system as the frequency gets higher. In the proposed system, according to the circuit model, in order to calculate the losses on the resistive part, the rms value of the current should be considered. The value of the rms current in a triangular waveform is given by the general equation of the rms current:

$$I_{rms} = \sqrt{\frac{1}{T}\int_0^T I^2(t)dt} \tag{3.53}$$

In the proposed system the major conduction losses come from certain components that have resistances that cannot be neglected. These resistances are from the series resistance of the solar cell and the resistances of the switches.

1. R_s
2. R_{sw1}
3. R_{sw2}

For all the above-mentioned resistances the current that flows is inductor current. For the switch, the current is flowing only when they are on. The power loss can be calculated by the following equation:

$$P = I_{rms}^2 R \tag{3.54}$$

The switching losses of the switches are caused due to the nonzero switching time of the semiconductor device. Current and voltage across a MOSFET transistor cannot switch from zero to the provided from the circuit value in zero time. The same is true also for the inverse case, meaning that MOSFET cannot switch in zero time from the provided value to zero both for current and voltage. So, this causes additional losses to the system. In Figure 3.10 a characteristic case is shown for a boost converter. Vg represents the voltage on the MOSFET.

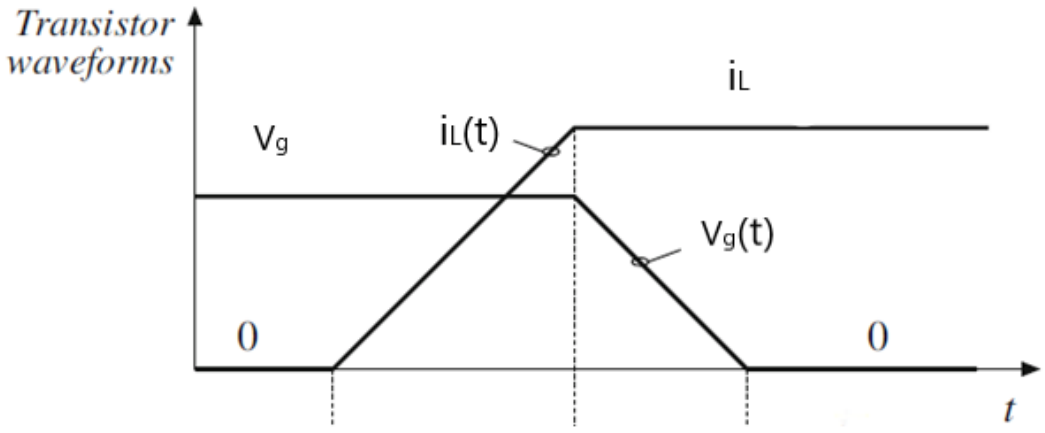

Figure 3.10: Transistor waveforms of a boost converter when the transistor turns on.[38]

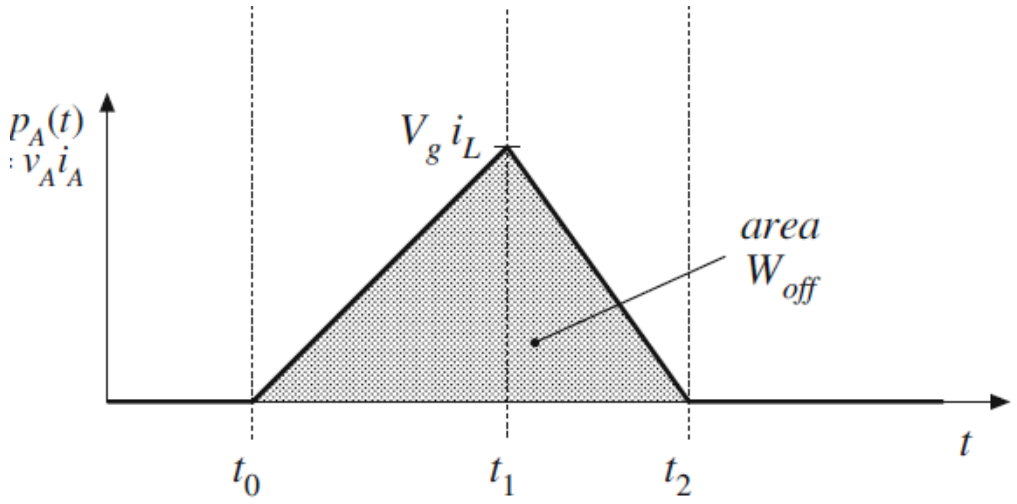

Figure 3.11: Power lost in a transition of a transistor.[38]

In Figure 3.11 is shown that the switch needs a very small amount of time to turn off. Similar time is also needed to turn on. A conservative estimation for this time is 0.01 times the switching period. The situation that the Figure 3.11 shows is the energy that is lost when the transistor is switching. An approximation to calculate these switching losses is to consider the current that flows through the MOSFET before the transition and the voltage across the MOSFET after the transition. The total transition time is $t_2 - t_1$. With this approximation that the waveforms are triangular the turn off switching losses are given by:

$$\mathrm{W_{off}} = 0.5 i_L V_g (t_2 - t_0) \tag{3.55}$$

The same methodology can be used to calculate the switching losses when the switch turns on. In this situation the current value should be the value after the transition and the voltage value should be the value before the transition 25]. Thus, the total switching losses are given by:

$$\mathrm{P_{swloss}} = \left(W_{off} + W_{on}\right) f_s \tag{3.56}$$

By considering all the above-mentioned losses, the efficiency of the system can be calculated according to the following equation:

$$efficiency = \frac{P_{in} - P_{Rs} - P_{sw1} - P_{sw2} - P_{swloss}}{P_{in}} \tag{3.57}$$

Where:

- P_{in} is the input power.
- P_{Rs} is the power that is lost in the series resistance.
- P_{sw1}, P_{sw2} are the power losses due to the transistor resistances.
- P_{swloss} is the power loss during the switching periods.

One important point to mention is that with this system, inductor core losses are limited to zero as there is no use of core. Core losses are significant losses in the total losses of an inductor.

Chapter 4: Simulation results

4.1 Simulation setup

The simulations have been carried out through MATLAB. Based on the fact that PV module made of 5-inch IBC solar cells is considered for this study, simulations have been carried out with 96 solar cells in series. In addition, the selection of the module is based on [39]. Different cases have been simulated, considering a PV module layout consisting of a total of 96 solar cells. Among these solar cells, some of them are referred as “special cells”. These are cells that are supposed to have higher inductance and resistance, for instance due to a redesign of their metallization or the addition of a spiral coil on their back. More special cells increase both the PV module inductance and resistance. Therefore, the current ripple as well as the overall efficiency will be affected by the number of special cells within the PV module. That is the reason why the different cases, summarized in Table 4.1, have been simulated. As a reference and as a mean to study the possibility of cell-level power conversion, also the case of a single-cell module made of a single special cell has been studied.

TABLE 4.1: Simulated PV module’s configurations

Number of solar cells in series	Number of special cells
1	1
96	96
96	48
96	32
96	16
96	12

A range of values have been considered for the simulations as the previous studies have different measurements for the parameters that are shown in Chapter 2. The minimum and maximum values of the additional resistance and inductance of the special cells have been calculated through the Finite Element Model (FEM) programme COMSOL Multiphysics. The table 4.2 shows the range of the values.

TABLE 4.2: Solar cell parameter values

Resistance of single solar cell	3-10 mΩ
Capacitance of single solar cell	0.1-1 μF
Inductance of a special cell	0.1-100 μH
Additional resistance for a special cell	5-10 mΩ

Based on the table 5.2 the total equivalent resistance, inductance and capacitance for a PV module with 96 solar cells in series for the five configurations of table 5.1 are calculated. They are summarized in Table 4.3.

TABLE 4.3: Total values for a PV module for the different simulated configurations

Solar cells in series	Special cells	Resistance (Ω)	Capacitance (nF)	Inductance(μH)
96	96	0.768-9.6	1.041-10.41	9.6-9600
96	48	0.528-5.28	1.041-10.41	4.8-4800
96	32	0.448-3.84	1.041-10.41	3.2-3200
96	16	0.368-2.4	1.041-10.41	1.6-1600
96	12	0.348-2.04	1.041-10.41	1.2-1200

For each of the five configurations presented in Table 4.3, different initial conditions have been given. More specifically, several values of frequency and output voltage were set for the simulations. In Table 4.4 all the different input parameters are shown.

TABLE 4.4: Different initial conditions of the simulations

Frequency (kHz)	Output voltage (V)
100	96
300	96
500	96
700	96
1000	96
1000	144
1000	192

The operational conditions and the parameters not listed in the previous tables are kept constant. They are shown in Table 4.5.

TABLE 4.5: Constant initial conditions of the simulations

Photocurrent	5A
Ideality factor	1.1
Shunt resistance	20Ω
MOSFET resistance	1mΩ
Output capacitance	1μF
Resistance of output capacitance	1mΩ
Solar cell saturation current	10nA

4.2 Single cell PV module

The ripple in the input voltage and in the inductor current have been studied. It is very crucial to begin the study with the ripple in inductor current and the input voltage so as to ensure the proper operation of the boost converter and also because the linearized models upon which the simulations are done is based on the assumption that the ripple is low (small-ripple approximation). The first simulations are done for a case of a one-cell PV module made of a single special cell with the parameters of Table 4.2. In Figure 4.1 the ripple in the input voltage for the different values of capacitance and inductance of the single cell is shown for different values of frequency and considering an output voltage of the boost converter equal to 96V. It is important to introduce the area of interest, which the area where the ripple is below 10%. As it referred above the model represents reality only for low values of ripple.

Inductance is affecting crucially the system as only after a specific value (around 10μH) the value of the ripple is getting lower than 10 percent. As expected, also the capacitance has a an effect on the ripple, with the ripple decreasing as the capacitance is increasing. This effect is more evident at high frequency. The value of resistance of the cell is 8mΩ. In Figure 4.2 the area of interest (from 10μH) is shown. The effect of the inductance is dominant in the ripple.

The graph in Figure 4.3 shows the input voltage ripple for the highest value of resistance which is 0.1Ω. According to the fig. 4.3 resistance affects the ripple of the system. Specifically, when compared to Figure 4.1, the ripple is almost one order of magnitude smaller. At the frequency of 1 MHz, ripple is always under 10%.

In Figure 4.4 area of interest is shown for the ripple in input voltage for the highest value of resistance. The graphs are very similar and follows the same trend. In all the figures below the effect of frequency is also dominant in the values of the ripple. As the frequency is increasing the value of ripple is decreasing significantly.

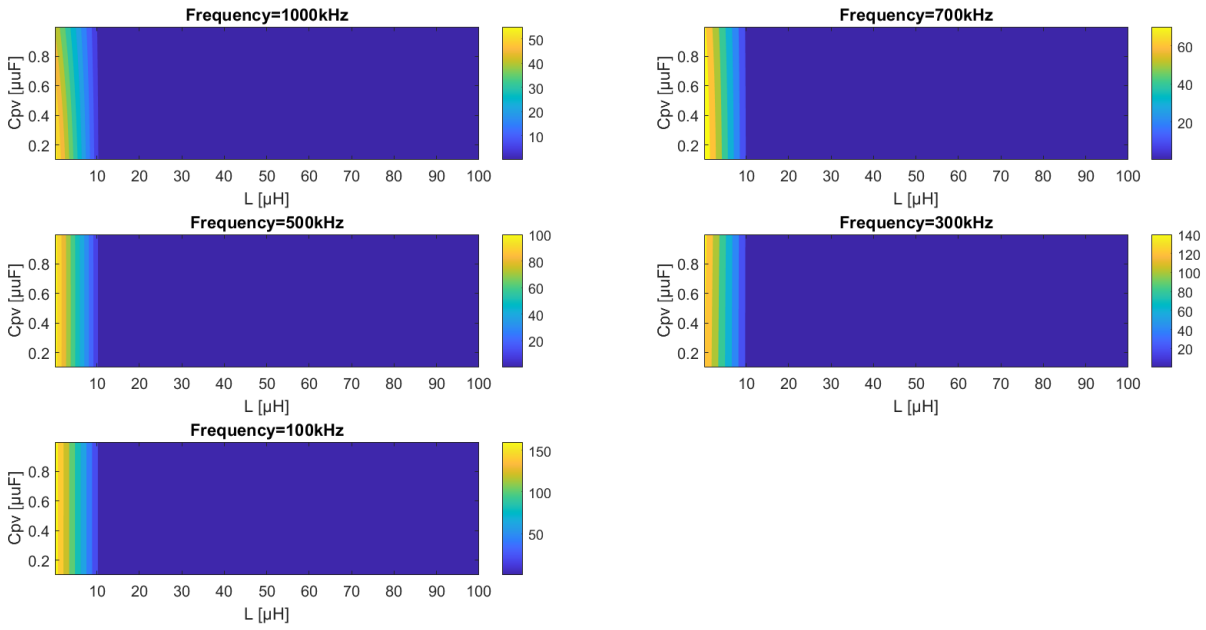

Figure 4.1: Input voltage ripple for the single-cell PV module with special cell's resistance equal to 8mΩ and output voltage of the converter equal to 96V

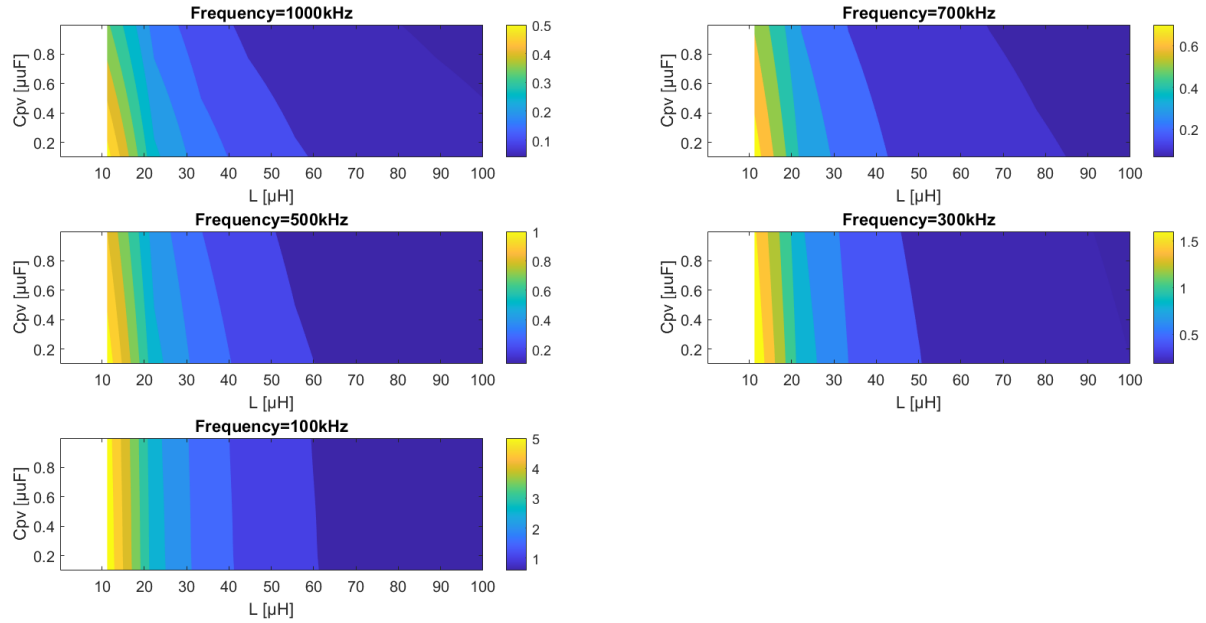

Figure 4.2: Input voltage ripple for the single-cell PV module with special cell's resistance equal to 8mΩ and output voltage of the converter equal to 96V at the area of interest

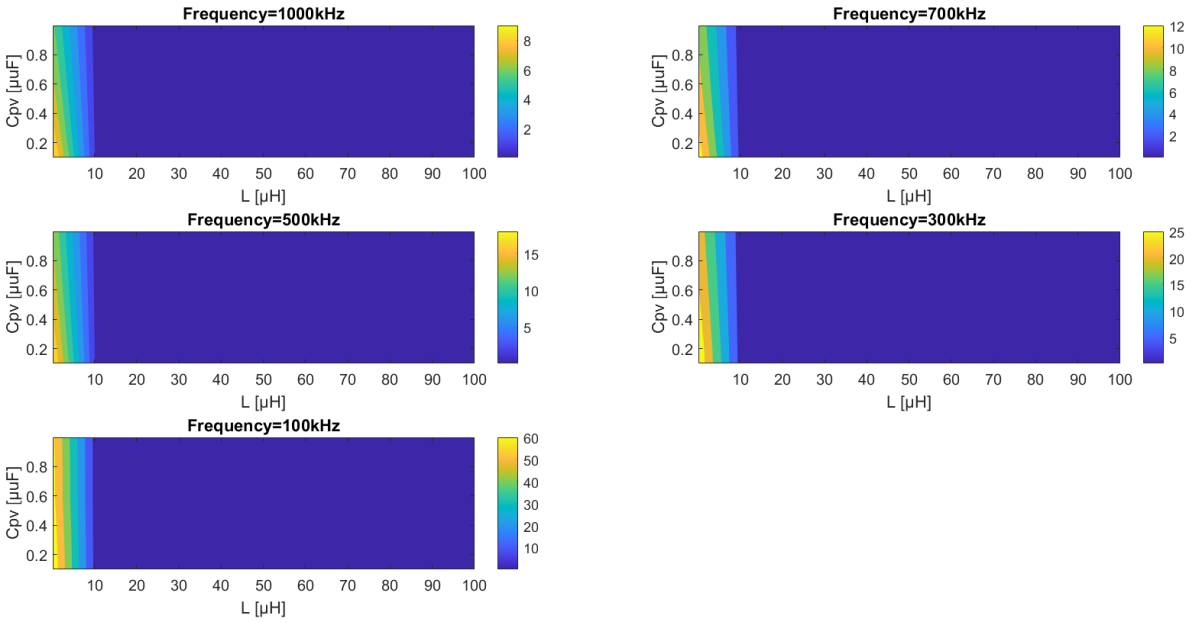

Figure 4.3: Input voltage ripple for the single-cell PV module with special cell's resistance equal to 0.1Ω and output voltage of the converter equal to 96V at the area of interest

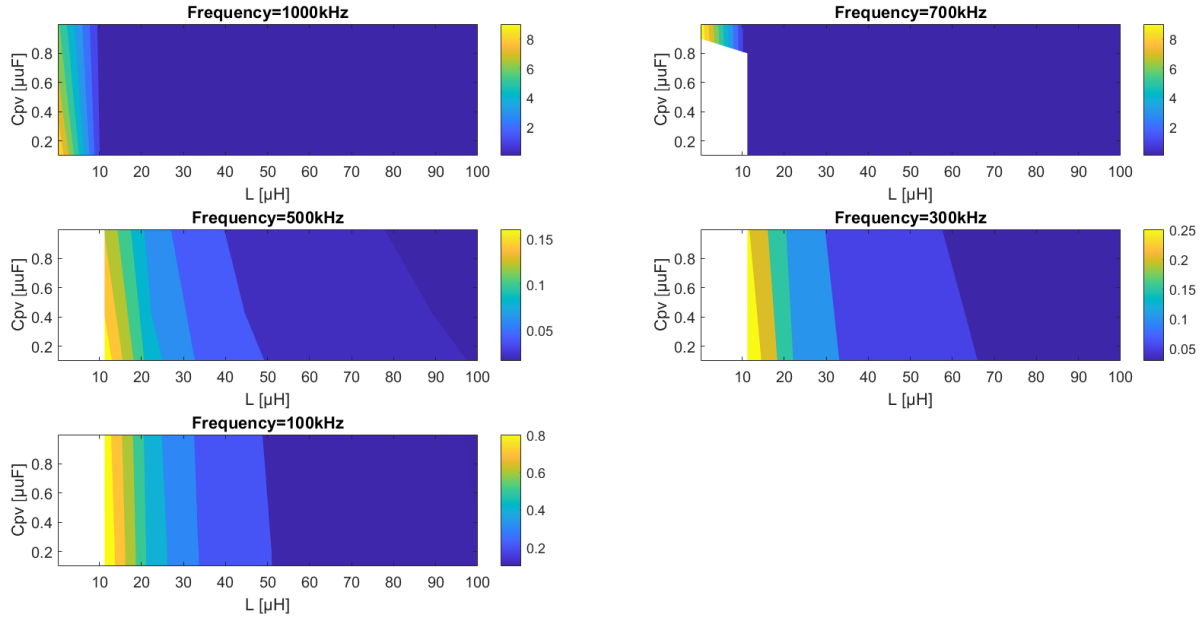

Figure 4.4: Input voltage ripple for the single-cell PV module with special cell's resistance equal to 0.1Ω and output voltage of the converter equal to 96V at the area of interest

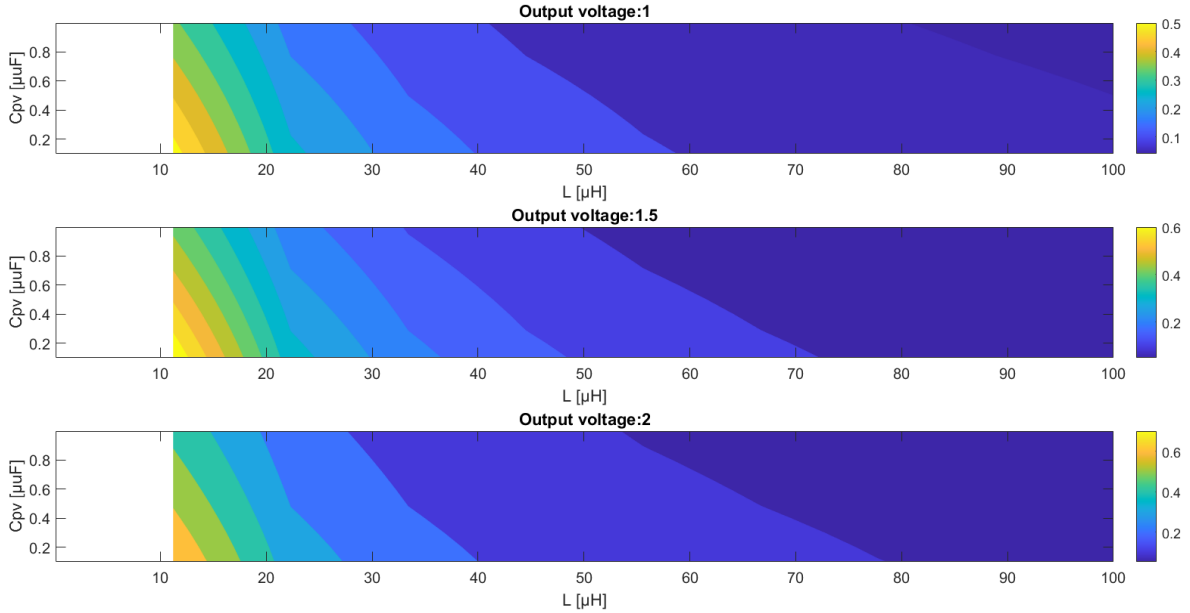

Figure 4.5: Input voltage ripple for the single-cell PV module with special cell's resistance equal to 0.008Ω and output voltage of the converter for 3 different output voltages at the area of interest

Simulations have been done for different values of the output voltage. In fig. 4.5 the contour plot shows how the output voltage affect the ripple in the input voltage. As the output voltage increases the ripple has a slight increase. Increase in the output voltage will lead to an increase in the duty cycle, so the ripple is affected also.

The same simulations have been done for the inductor current ripple. In Figure 4.6 the values of the ripple are shown for the different ranges of inductance and capacitance. The graph is only at the area of interest as before. Usually inductor current ripple can be higher compared to the input voltage ripple. The area of interest in this case is set under 20%.

Frequency has also the same effect in the inductor current ripple (same with the input voltage ripple) and as it is increasing it lowers the ripple. Based on the Figure 4.6 the inductance has the most dominant role in the value of the inductor current ripple as after 10μH the ripple is very low. Increase in the capacitance as it shown in the Figure 4.6 is not affecting at all the value of the inductor current ripple.

Simulations have been done also for the other values of resistance. Figure 4.7 shows the inductor current ripple for the highest value of the resistance. Also, in this case inductance is playing the dominant role for the change in the ripple. Comparing Figure 4.6 with Figure 4.7 the increase in resistance lowers the value of inductor current ripple. In the case of Figure 4.7 all values of ripple are under 20% for 1000kHz and 700kHz

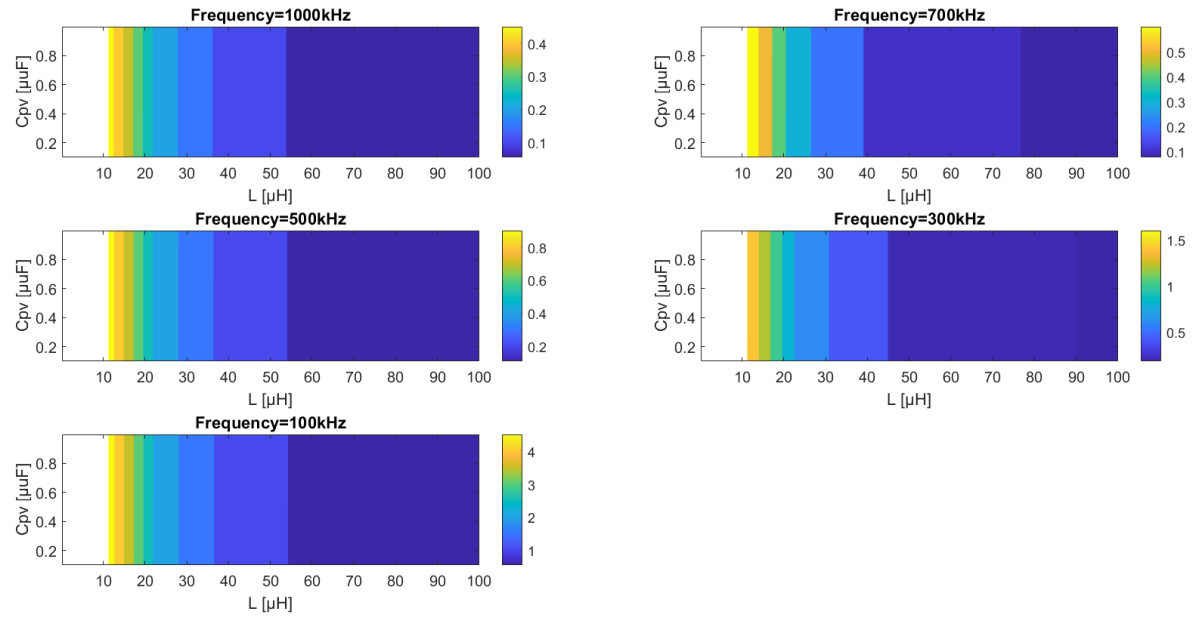

Figure 4.6: Inductor current ripple for the single-cell PV module with special cell's resistance equal to 8mΩ and output voltage of the converter equal to 96V at the area of interest

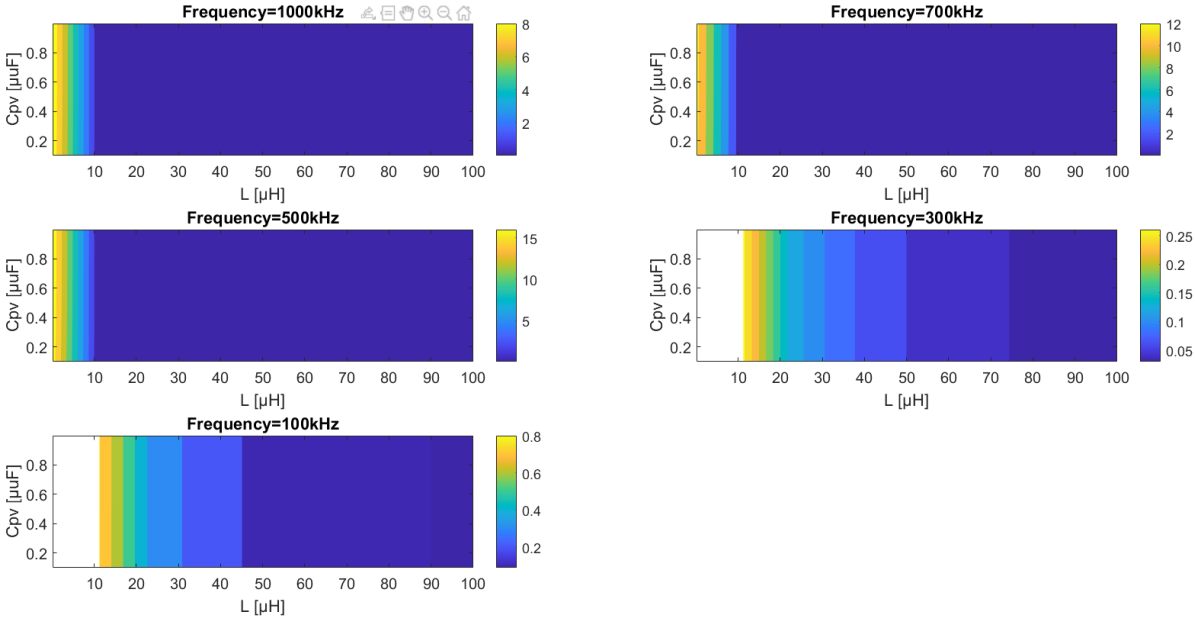

Figure 4.7: Inductor current ripple for the single-cell PV module with special cell's resistance equal to 0.1Ω and output voltage of the converter equal to 96V at the area of interest

In Fig 4.8 results of the simulations for different output voltage values are shown. Increase in the output voltage is almost not affecting the value of the inductor current (same as in the ripple in the input volage).

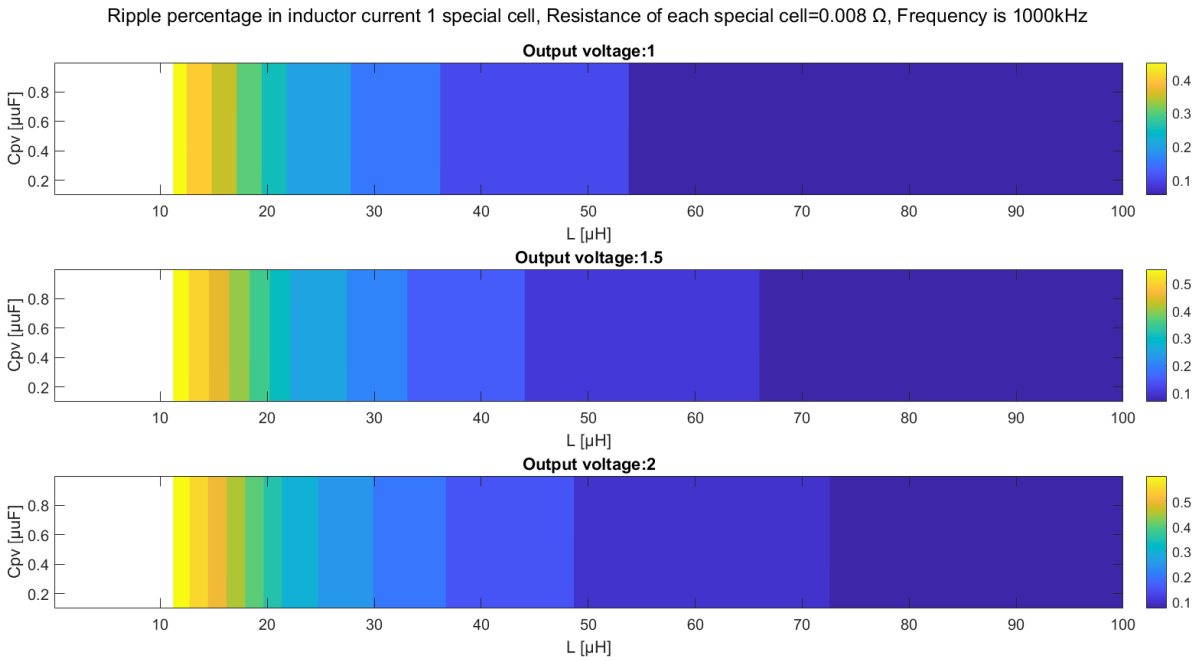

Figure 4.8: Inductor current ripple for the single-cell PV module with special cell's resistance equal to 0.008Ω and output voltage of the converter for 3 different output voltages at the area of interest

According to the previous results, inductance and frequency affect the ripple in the input voltage and the inductor current significantly compared to all the other parameters of the system. Another important conclusion is that after a certain value of inductance (around 10μH) the value of ripple for both the input voltage and the inductor current is lower from the limits that were set (5% for input voltage and 20% for inductor current). This means that the area of interest (where the system represents reallity) is over 10μH.

In addtion to the ripple, another very important parameter of the system that should be simulated and studied is the efficiency. The efficiency is calculated as shown in Chapter 4 As expected and confirmed by the results of the simulations, efficiency is mostly affected by the value of the resistance. In Figure 4.9 the efficiency as a function of the resistance is presented.The shaded area is the range of the efficiency (as the capacitance and inductance changes). In high frequency is obvious that almost only resistance affects the efficiency (effect of the inductance and capacitance is negligible). From the graph it can be extracted that the relation is almost linear between the resistance and the efficiency, but in all cases efficieny can not exceed 80%.

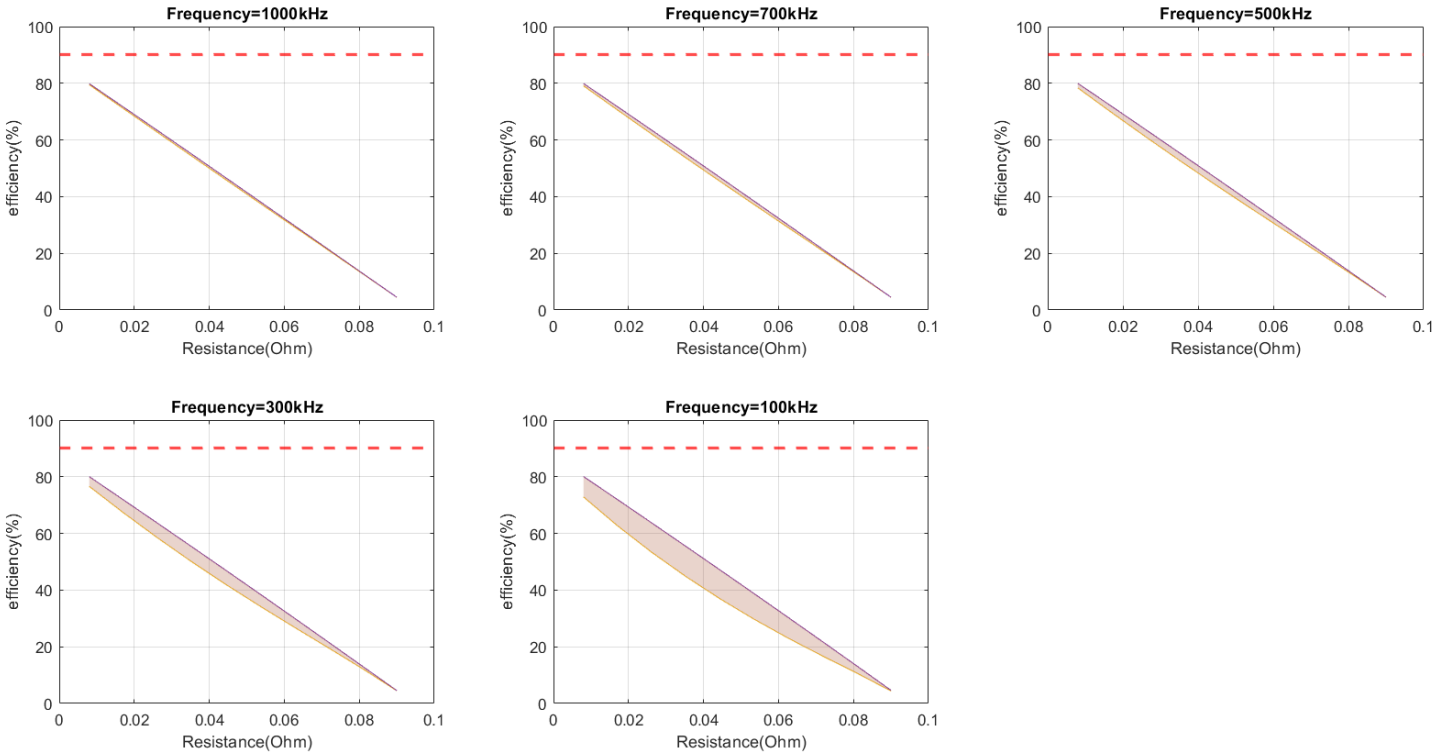

Fig 4.9: Efficiency of the one-special-cell PV module for different values of resistance with output voltage of the converter equal to 96 V.

4.3 96-cell PV module

The next part of simulations has been done for a PV module with 96 solar cells as shown in Table 4.1. In the next figures results of the 12 special cells case will be shown. The trends of the other cases is same as the case of 12 special cells that will be presented. The red line in the ripple figures is the highest accepted value and is set to 5% for the input voltage and 20% for inductor current. The red line in the figures of efficiency is the accepted value and is set to 90%.

In Figure 4.10 the range in the input voltage versus the capacitance is presented. The shaded area is the range of the ripple based on the maximum and minimum value for each value of capacitance (both inductance and resistance change in the whole range).

In Figure 4.11 the variation of the input voltage ripple as a function of the inductance is presented. The x-axis represents the total inductance of the PV module, as shown in Table 4.3. The shaded area again is the range of the ripple based on the maximum and minimum value for each value of inductance. Comparing the two graphs inductance is affecting more the ripple than capacitance as it was shown also in the simulation results of one solar cell. It is important to mention again that the system needs to have low value of ripple so as to represent reality.

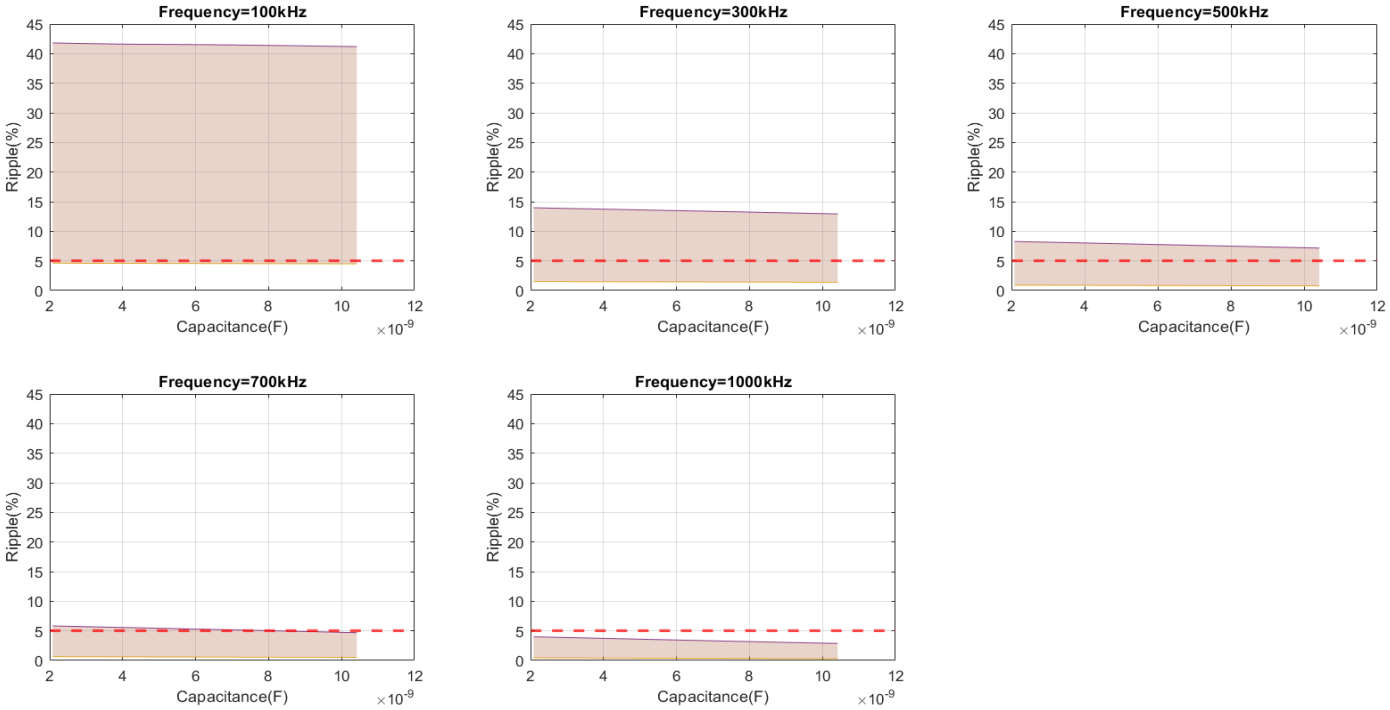

Fi gure 4.10: Range in the input voltage ripple versus the capacitance. Output voltage equal to 96V.

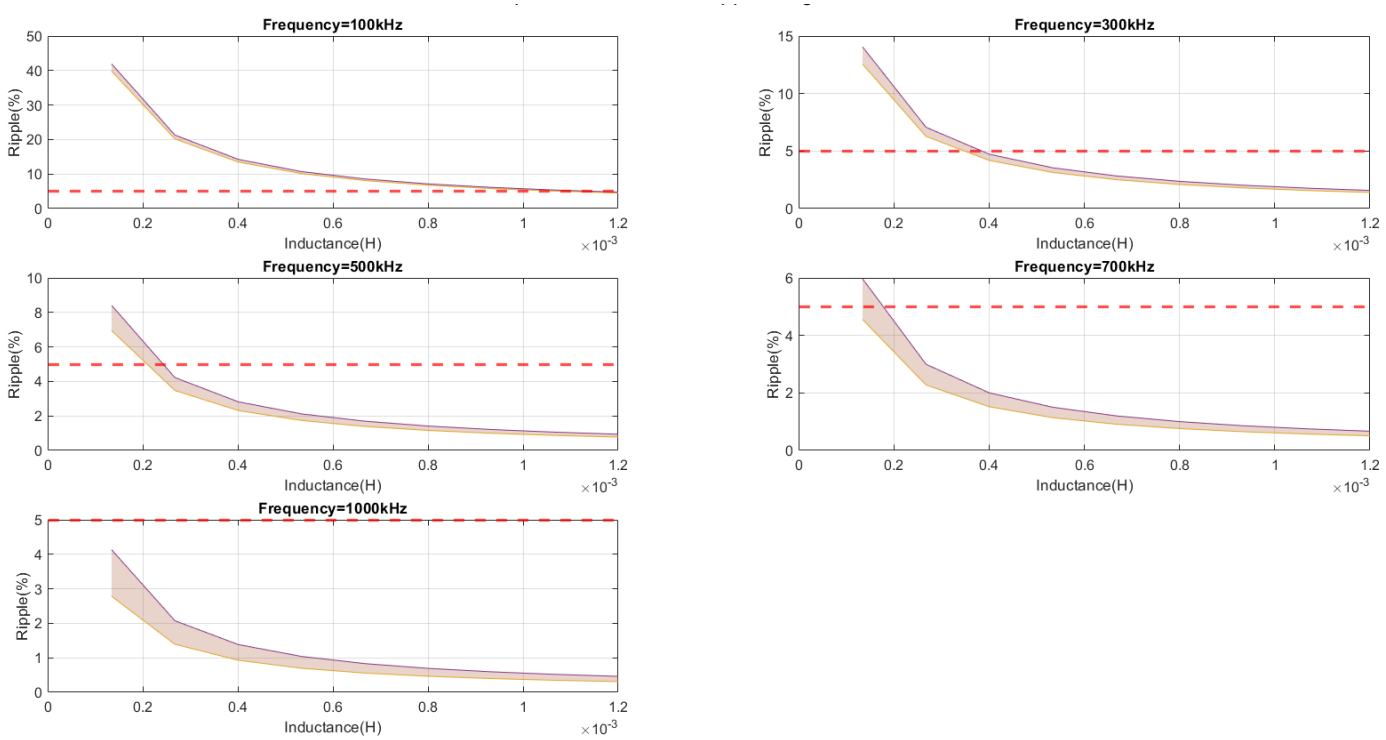

Figure 4.11: Range in the input voltage ripple versus the inductance. Output voltage equal to 96V.

From Figure 4.10 and Figure 4.11 is obvious that the ripple in input voltage for the case of a PV module with 96 cells where 12 are special cells is not able to achieve 5%. Also, comparing the two graphs values of inductance have a smaller shaded area of values of ripple (the range in the graphs is because one parameter is constant and the other parameters change). Interestingly, when the switching frequency increases, many of the simulated variations of parameters (triplets of inductance, capacitance and resistance values) become acceptable. It is worth to mention that the graphs in Figures 4.10 and 4.11 do not include the lowest value of inductance as the ripple is very high for such a small inductance as shown in Figure 4.12. The Figure 4.13 shows only the input voltage ripple, but the same happens also for the inductor current ripple.

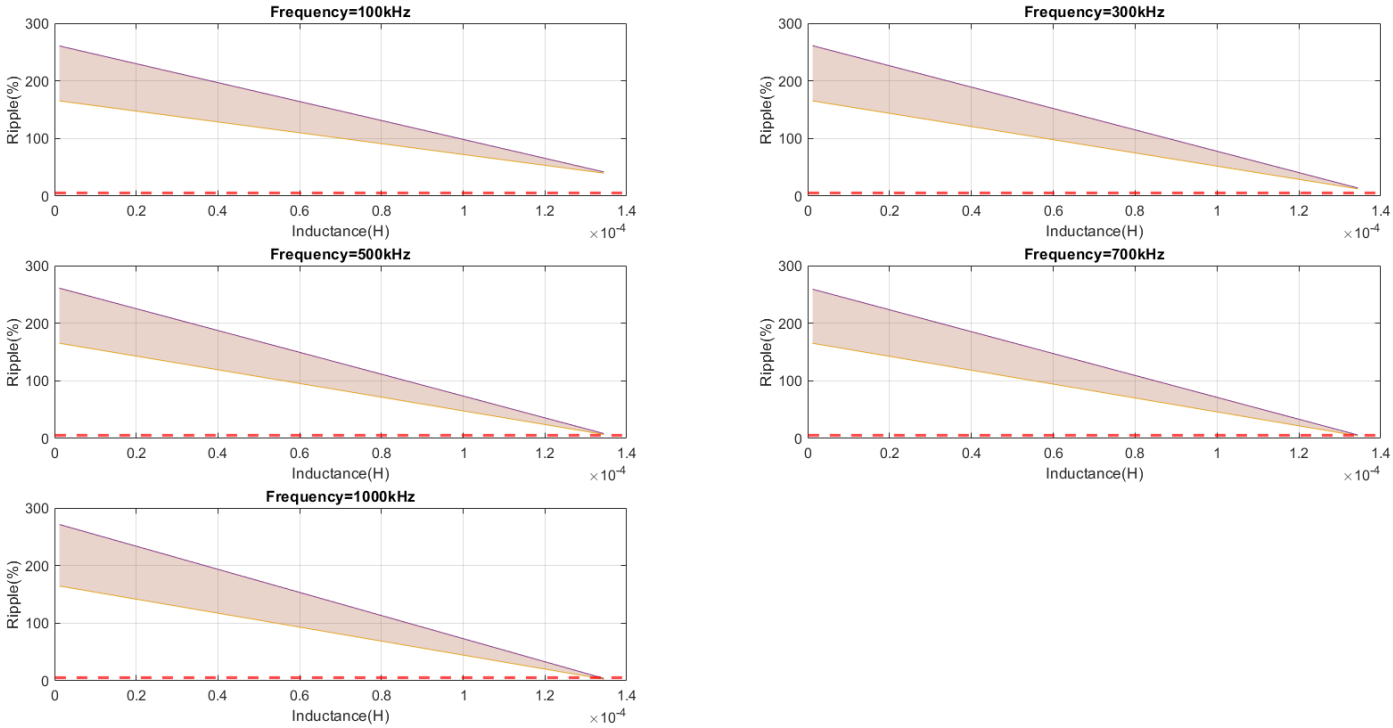

Figure 4.12: The range in the input voltage ripple at the lowest values of inductance. Output voltage equal to 96V.

In Figure 4.10, the capacitance does not seem to affect the ripple significanlty as with its change, there is no important change in the ripple. Inducrtance and frequency significantly lower the input voltage ripple based on these results.

In Figure 4.13 simulations results are shown for a change in the output voltage (92V,144V,192V). The results indicate that there is a slight increase in the ripple but rarely above the limit of 5%. This leads to the conclusion that output voltage until the simulated value of 192V is not an obstacle for the ripple of the system.

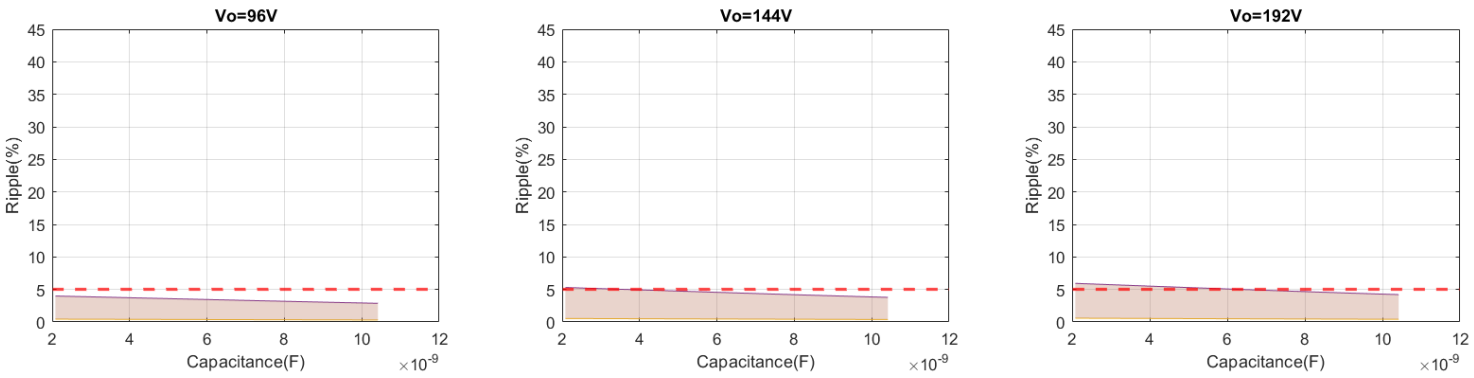

Figure 4.13: Range in the input voltage versus the capacitance for different values of output voltage.

Based on the previous figures, as the frequency and the inductance increase, there are more acceptable values of ripple. Also, as the capacitance is increasing the ripple becomes lower, but within the considered range of variation it has a slighter effect (the range of variation of capacitance is one order of magnitude compared to inductance which is three orders of magnitude). As it is referred above when discussing Figure 4.10 and Figure 4.13, the shaded area is the range between the maximum and the minimum value of the ripple for the specific values of capacitance. This means that for a specific value of capacitance there can be accepted and non-accepted values for the ripple as inductance and resistance change.

Being more specific on the results, for the simulation of 100kHz there is no acceptable value of ripple and for the case of 1000kHz all the values of ripple are accepted. This shows that as expected the switching frequency of the system strongly affects the performance.

The second parameter that was studied was the ripple in the inductor current. This parameter is also important as the previous one as it should be low to represent the mathematical model. In Figure 4.14 the results of the ripple in the inductor current are shown for the five different values of frequency considering an output voltage equal to 96V. The red dashed line here is also the limit of the maximum accepted ripple that has been set and is 20%. Boost converters are designed to have higher inductor current ripple [].

In Figure 4.15 the ripple in the inductor current was simulated for the different values of output voltage and switching frequency equal to 1MHz. Both Figure 4.14 and Figure 4.15 x-axis is the inductance as it is the parameter that affects the most the ripple in the inductor current, as demonstrated by the negligible shaded area.

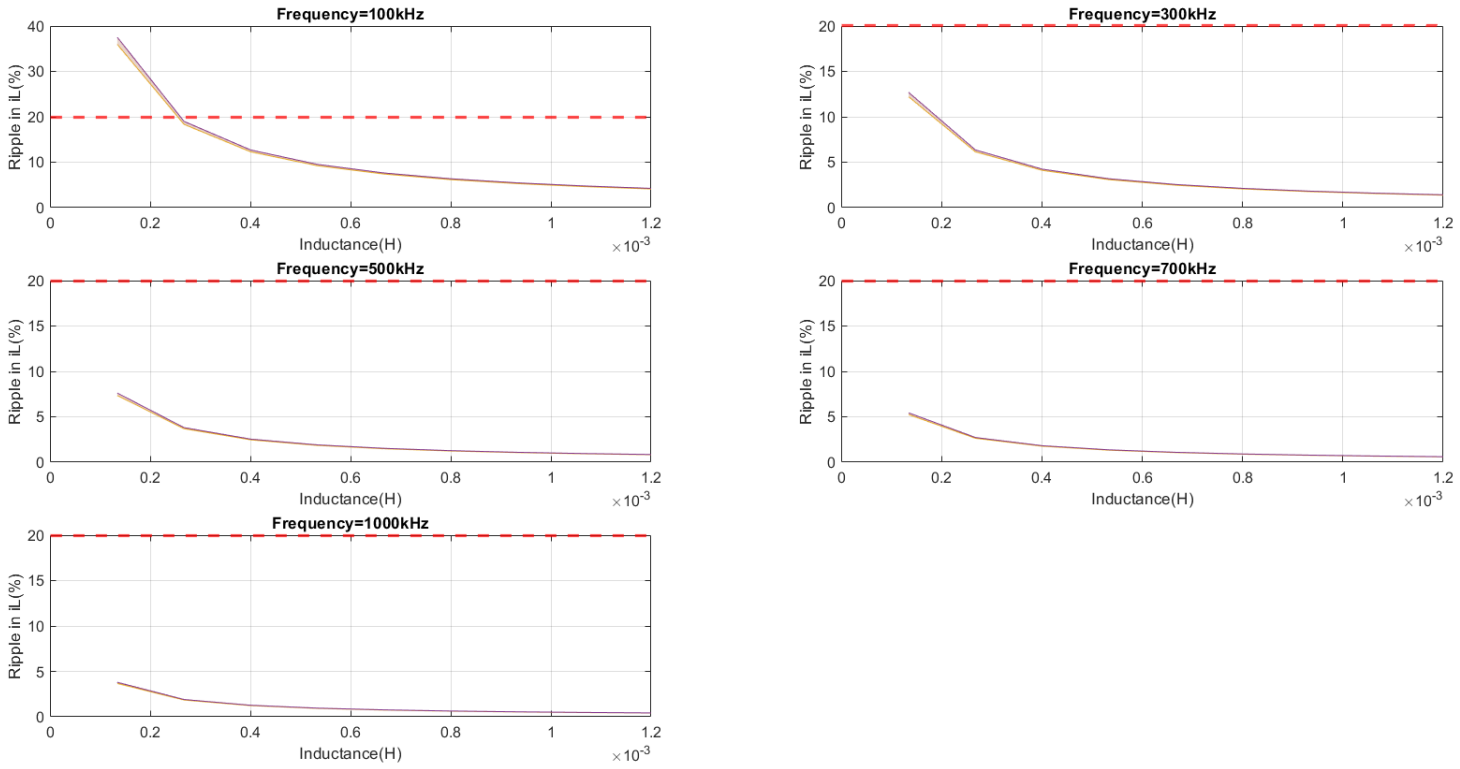

Figure 4.14: Ripple in inductor current for 12 special cells module for different values of frequency.

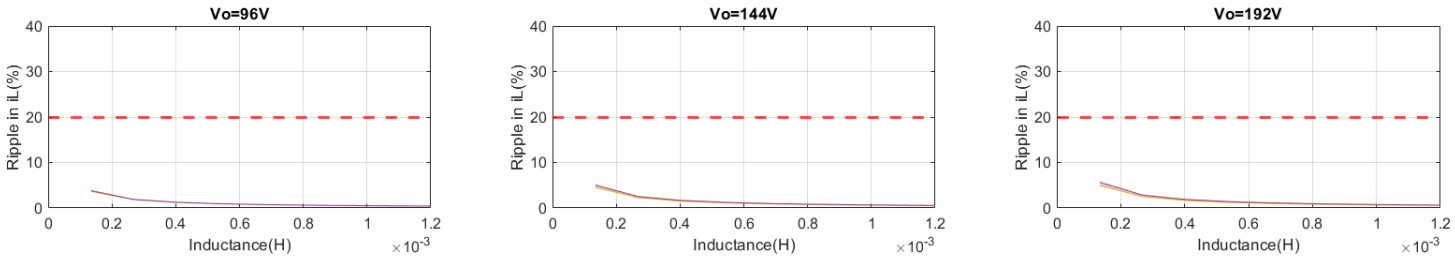

Figure 4.15: Ripple in input voltage for 12 special cells module for different values of output voltage.

In comparison with the ripple in the input voltage at 100kHz there few values of ripple for the inductor current that are accepted as the limit is 20%. Moreover, as the frequency increases the ripple in the inductor current is under 20% independent of the inductance.

Considering the change in the output voltage in Figure 4.15, the effect in the ripple is not so obvious as it seems to increase the ripple in the cases where the inductance is lower but all the cases are accepted based on the limit of 20%.

The third part of the simulations for the 96-cell PV module was the efficiency of the system. The way that was calculated is explained in Chapter 3. In Figure 4.16 the efficiency of the system with the increase in resistance is shown for several values of frequency.

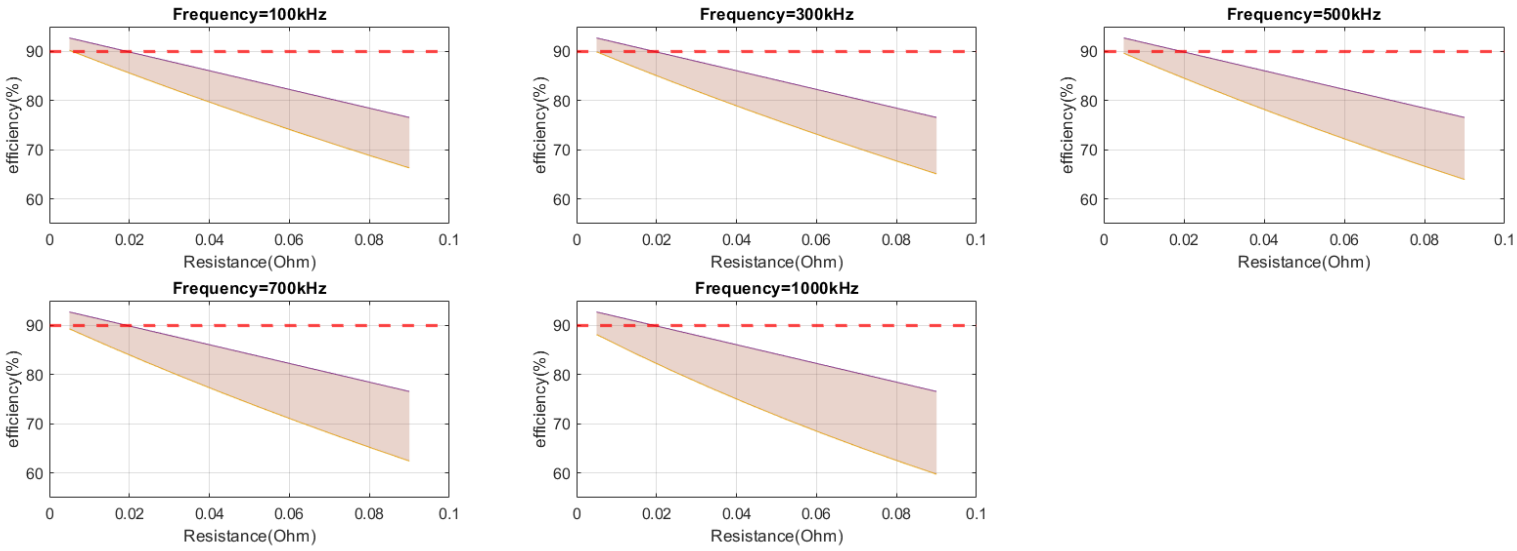

Figure 4.16: Efficiency of the system for different values of frequency.

The red dashed line has been set to 90% so as the efficiency of the system can be comparable with a conventional *smart* PV module, that is a PV module with an integrated DC-DC optimizer. Figure 4.16 shows that there is an almost linear corelation between the efficiency and the resistance of the system. It is remarkable that for most of the values of the resistance, efficiency cannot exceed 90%. In Figure 4.17 the efficiency was simulated for the different values of output voltage.

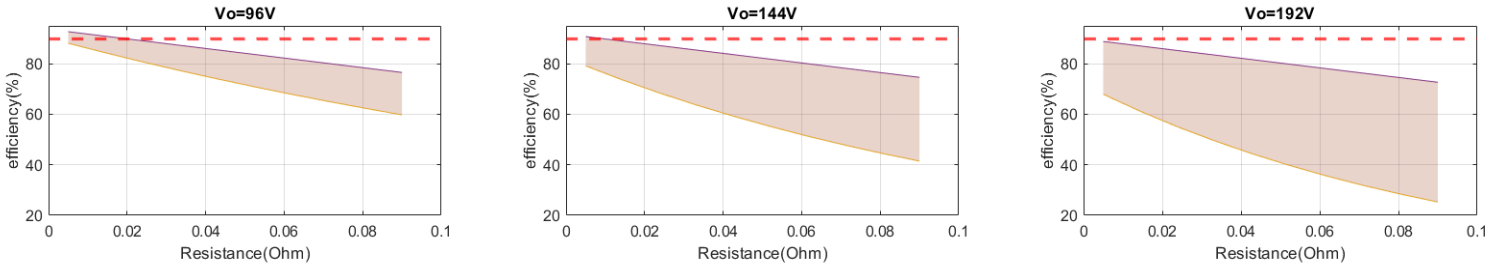

.

Figure 4.17: Efficiency of the system for different values of output voltage.

According to the simulations that have been done, the most dominant factor that affects the efficiency of the system is, as expected, the total resistance. However, also the inductance and capacitance do have a clear effect on the efficiency, as shown by the wide shaded areas in Figures 4.16 and 4.17. From the Figure 4.16 it can be observed that the efficiency can exceed the value of 90% percent for very few and very small values of resistance.

On the other hand, the change in the output voltage make a difference in the total efficiency as the converter needs to work with higher duty cycle. Both in the cases of 144V and 192V there is almost no value of efficiency over 90%. Another conclusion in Figure 4.17 is that as the output voltage increases, the effect of inductance and capacitance affect the efficiency as the shaded area is increasing.

For the other PV module's configurations summarized in Table 4.1, the trend of the graphs is very similar. The significant difference is in the efficiency of the system as the resistance is getting bigger and bigger with the increase of the number of special cells. The ripple both in input voltage and inductor current is low when the value of inductance in over the medium value of its range. In Figure 4.18 the efficiency of the system is presented for the different PV module's configurations, with a switching frequency of 1 MHz and a converter output voltage of 96V. In the case of 96 special cells, all the values of efficiency are below the limit of 90%. This leads to the fact that the 96 special cells case can have the best performance in terms of ripple, as the inductance will be higher, but the efficiency of the system cannot achieve the set limit value. Another important remark is that, in all cases, efficiency can be above the set limit of 90% only for very small values of resistance. Therefore, the additional resistance of each special cell cannot be high. In Figure 4.19 is indicated the efficiency versus the value of resistance of each special cell for the cases of Table 4.1

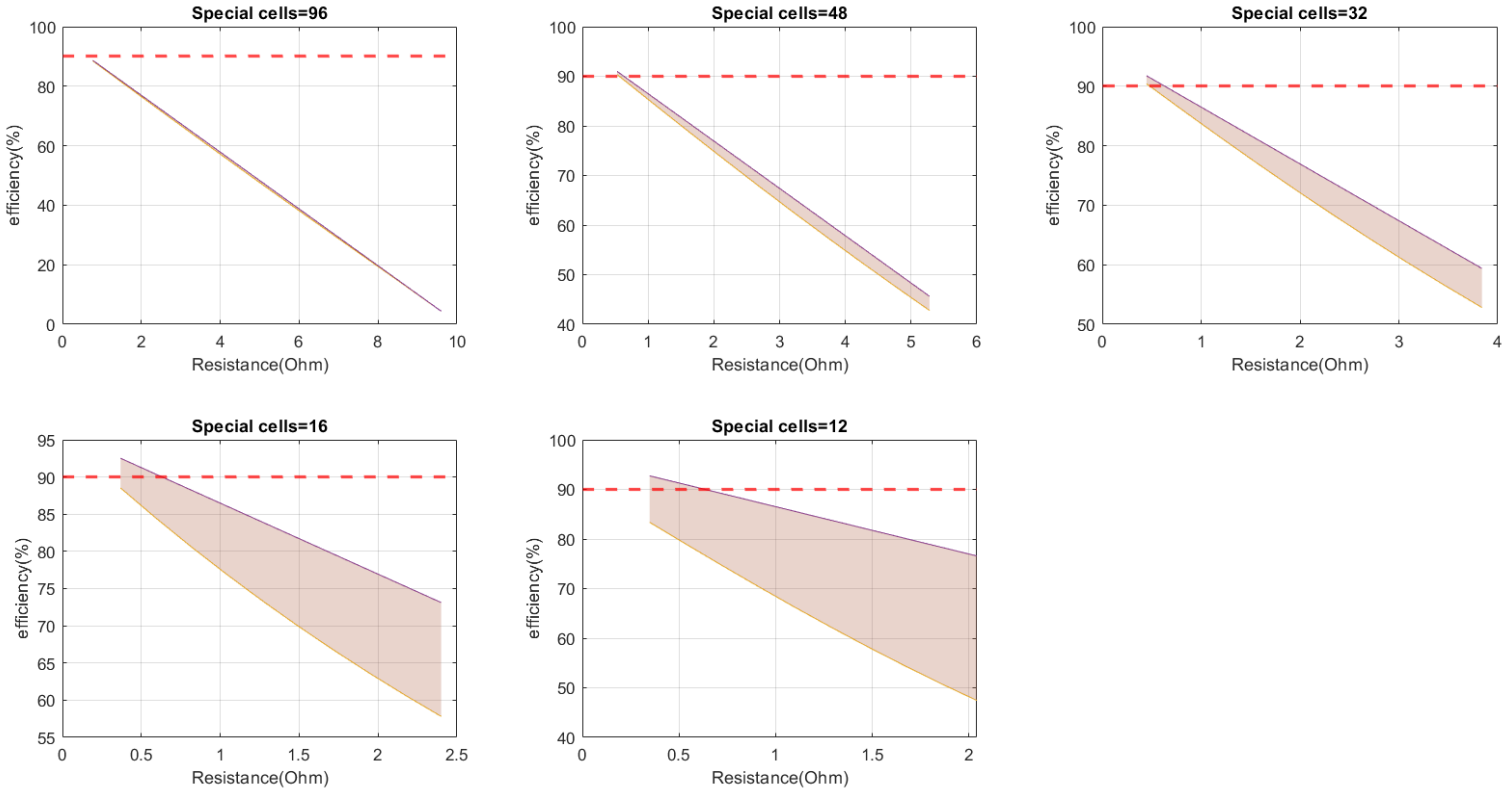

Figure 4.18: Efficiency of the system for the different cases of special cell.

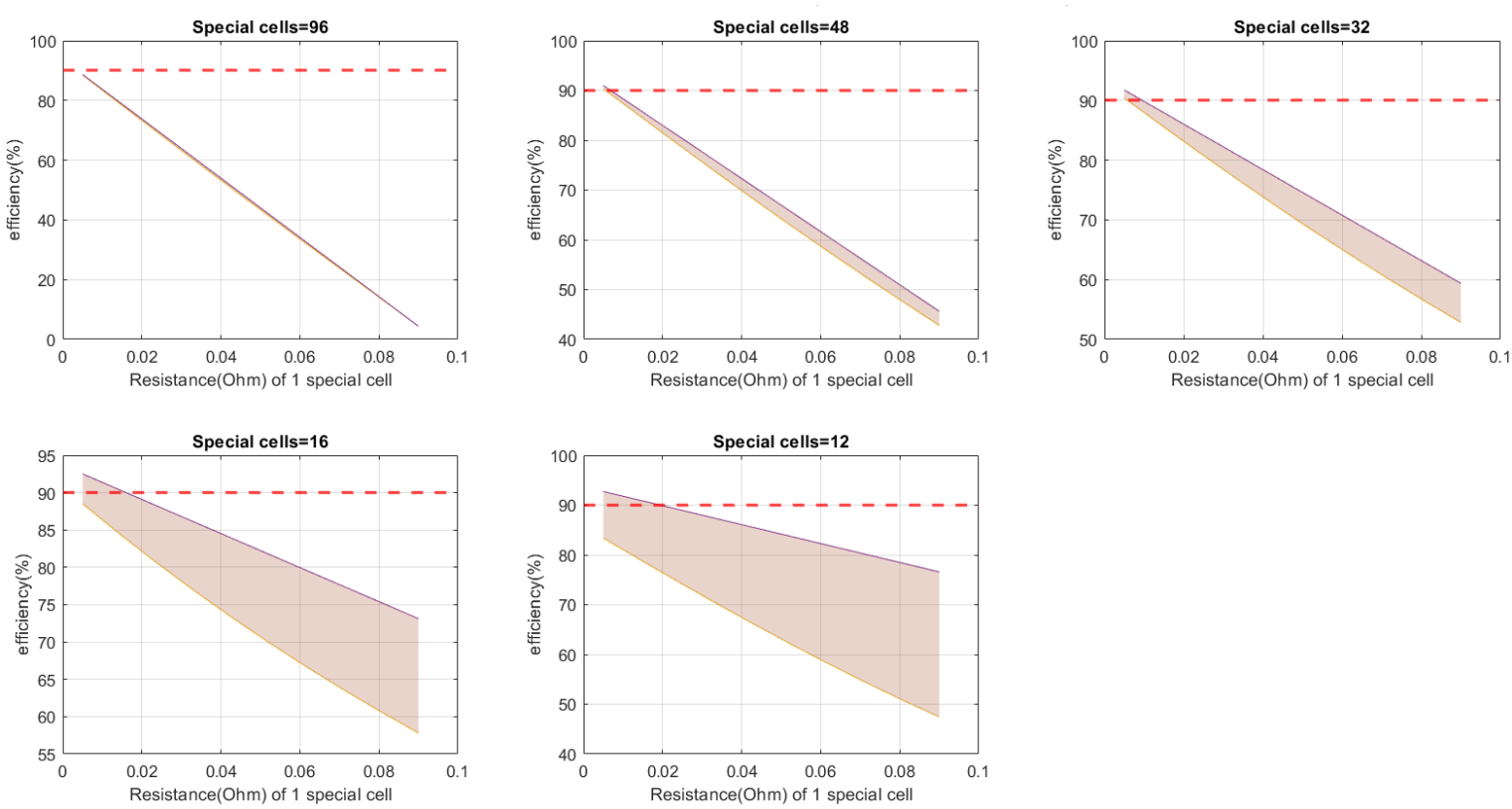

Figure 4.19: Efficiency versus the value of resistance of each special cell.

Chapter 5: Discussion and conclusions

Considering the results of the simulations, general conclusions for the proposed system can be that for the ripple behaviour inductance and frequency have the most dominant role. Both increase in these values lead to significant decrease in the input voltage and inductor current ripple. Beginning with the single solar cell case, in most cases the ripple in the input voltage and inductor current is lower than 10% when the value of inductance is over 10μH.

From Figure 4.2, which the area of interest (ripple under 10%), the input voltage ripple is slightly affected by the capacitance and from Figure 4.6, the inductor current ripple is almost not affected by it. This lead to the conclusion that capacitance affects in a significant way only the input voltage ripple and has very limited effect on the inductor current ripple. On the other hand, comparing Figure 4.2 with Figure 4.4 and Figure 4.6 with Figure 4.7, increase in the resistance seems to lower the ripple both in input voltage and inductor current up to an order of magnitude in some cases, which is a significant decrease. Output voltage is not an important factor for the performance of the system in both cases of ripple.

Efficiency of the system seem to have a linear corelation to the resistance. Specifically in Figure 4.9 in the high frequency cases, inductance and capacitance are not influencing the efficiency as the shaded area between the maximum and the minimum values of it for the specific values of resistance is very small. In the low frequency inductance and capacitance are affecting the system more. Another important remark is that in the high frequency simulation results the maximum efficiency is little degraded, and this is due to the switching losses.

In terms of the case of 96-cell PV module with 12 special cells, the results of the simulation follows the same trend as in the case of one single cell. Input voltage ripple is mostly affected by the values of inductance and frequency. In Figure 4.10 increase in the capacitance, especially in the low frequency case is almost not changing the value of the ripple. Comparing Figure 4.10 with Figure 4.11, inductance has dominant effect on the ripple. In the results of the inductor current ripple, influence of the inductance is more dominant, which is the same as in the case of the single cell. This is happening also because of the range of values studied for the capacitance and inductance. For the capacitance, the range of the values varies of one order of magnitude and for the inductance it varies of about three orders of magnitude. Studying the result of an increase in the output voltage for the ripple in both input voltage and inductor current, they are almost not affected.

For the results of the efficiency, there is again a linear correlation with the resistance but comparing this case with the single cell, inductance and capacitance seem to affect the system more as the shaded area is greater. Output voltage is not affecting the maximum value of the efficiency based on the results in the Figure 4.17, but it significantly lowers the minimum value for each specific resistance.

From Figure 4.18, as the special cells are increasing the value of efficiency is decreasing. This is happening because the value of the whole resistance of the system is getting very high. Another important remark is that in the cases of 96 and 48 special cells the efficiency is almost

bever above the accepted value of 90%. This leads to the conclusion that the system should not have more than 32 special cells.

Another significant element that should be mentioned is that the inductance and resistance have a corelation based on the design of the special cells. It is not realistic to have very low values of resistance and very high values of inductance. From the results it seems that inductance should be over 15μH so as the input voltage ripple is under 5%. In addition, the value of the resistance of each special cell should lower than 0.02Ω and only the for the case of 12 special cells.

It is important to determine ranges of the several parameters of the system so as to work properly. In Table 5.1 these ranges are shown based on the results that are presented on Chapter 4 for the configuration of 12 special cells. In Table 5.2 values of inductance and resistance are presented for each special cell.

TABLE 5.1: Range of the crucial parameters of the PV module

Inductance	>0.15mH
Frequency	>300kHz
Resistance	<0.5Ω

TABLE 5.2: Range of the crucial parameters for each special cell of the PV module

Inductance	>17μH
Resistance	<20mΩ

The last part of this study is the comparison between the proposed system and a conventional system made of a PV module with an embedded DC-DC converter. Based on the measurements made by the company SolarEdge, their DC-DC converters can achieve around 99% efficiency at 250W power, which the input power in the simulations of the study. Figure 5.1 shows typical efficiencies of SolarEdge converters for different input power.

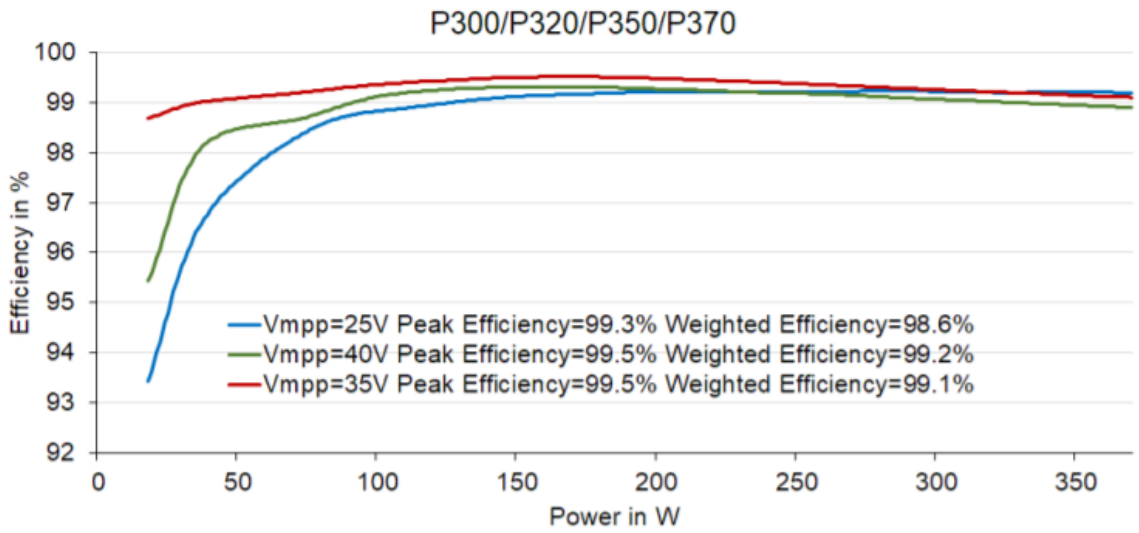

Figure 5.1: Conversion efficiencies of SolarEdge optimizers.[40]

The proposed system of this study can achieve 93% efficiency which is significantly lower than the SolarEdge DC-DC converters. The important difference in the comparison with the efficiency in the SolarEdge converters is that the efficiency calculated in this study include the whole module series resistance in the losses. This lead to extra conduction losses that are not accounted for in the evaluation of the efficiency of conventional power optimizers.

Future work can be done on different DC-DC converters as in this study the boost converter is analysed. SEPIC and buck-boost can be choices for further research. In addition, other ranges of the special cell parameter values can be examined. The range of the values in the simulations is linearly spaced and when passing from the first and smallest value of inductance to the second value, an important low-inductance range is missing that should be explored. It is very important to examine the aforementioned range as it critical to determine the minimum values of inductance that ripple is under the set limits. Moreover, a new model can be designed for the conventional system fairly compare it to the proposed solution.

References

[1] RITCHIE, Hannah; ROSER, Energy. *Our world in data*, 2020.

[2] RITCHIE, Hannah; ROSER, Max. CO_2 and greenhouse gas emissions. *Our world in data*, 2020.

[3] IEA, "World Energy Outlook – Topics," *IEA*, 01-Oct-2021. [Online]. Available: https://www.iea.org/topics/world-energy-outlook. [Accessed: 16-Dec-2021].

[4] LAFOND, François, et al. How well do experience curves predict technological progress? A method for making distributional forecasts. *Technological Forecasting and Social Change*, 2018, 128: 104-117.

[5] UNDELAND, Mohan N.; ROBBINS, Wiliam P.; MOHAN, N. Power electronics. In: *Converters, Applications, and Design*. John Whiley & Sons, 1995.

[6] HAQUE, Ahteshamul. Maximum power point tracking (MPPT) scheme for solar photovoltaic system. *Energy Technology & Policy*, 2014, 1.1: 115-122.

[7] SMETS, Arno HM, et al. *Solar Energy: The physics and engineering of photovoltaic conversion, technologies and systems*. UIT Cambridge, 2015.

[8] PRIYA, S.; UPPARA, Rajesh. Renewable Energy Fed BLDC Motor with DC-DC Converter by Implementing MPPT Technique for EV Application.

[9] ARGYROU, Maria C., et al. A grid-connected photovoltaic system: Mathematical modeling using MATLAB/Simulink. In: *2017 52nd International Universities Power Engineering Conference (UPEC)*. IEEE, 2017. p. 1-6.

[10] ABRAMOVITZ, Alexander; SHMILOVITZ, Doron. Short Survey of Architectures of Photovoltaic Arrays for Solar Power Generation Systems. *Energies*, 2021, 14.16: 4917.

[11] WANG, Feng, et al. Submodule level distributed maximum power point tracking PV optimizer with an integrated architecture. *Journal of Power Electronics*, 2017, 17.5: 1308-1316.

[12] OLALLA, Carlos, et al. Architecture and control of PV modules with submodule integrated converters. In: *2012 IEEE 13th Workshop on Control and Modeling for Power Electronics (COMPEL)*. IEEE, 2012. p. 1-6.

[13] PILAWA-PODGURSKI, Robert CN; PERREAULT, David J. Submodule integrated distributed maximum power point tracking for solar photovoltaic applications. *IEEE Transactions on Power Electronics*, 2012, 28.6: 2957-2967.

[14] https://www.solaredge.com/. Last accessed 16/12/2021.

[15] https://www.taylor-energy.com/. Last accessed 16/12/2021.

[16] http://www.zerun-tech.com/. Last accessed 16/12/2021.

[17] https://www.maximintegrated.com/en.html. Last accessed 16/12/2021.

[18] "Solar Cell Optimizer Technology | Maxim Integrated", *Maximintegrated.com*, 2021.

[19] "Why choose smart modules? ", solgen.pl/technologia-smart/. Last accessed 16/12/2021.

[20] NEAMEN, Donald A. Semiconductor physics and devices: Basic principles, Richard D. Irwin. *Inc., Boston*, 1992.

[21] T. Tektronix et al., "Tektronix Test & Measurement Solutions", *Tek.com*, 2021.

[22] MERHEJ, P.; DALLAGO, E.; FINARELLI, D. Effect of capacitance on the output characteristics of solar cells. In: *6th Conference on Ph. D. Research in Microelectronics & Electronics*. IEEE, 2010. p. 1-4.
[23] COTFAS, Petru Adrian, et al. Solar cell capacitance determination based on an RLC resonant circuit. *Energies*, 2018, 11.3: 672.
[24] GHANI, Faisal; DUKE, Mike; CARSON, J. Numerical calculation of series and shunt resistances and diode quality factor of a photovoltaic cell using the Lambert W-function. *Solar Energy*, 2013, 91: 422-431.
[25] ALRASHIDI, M. R., et al. A new estimation approach for determining the I–V characteristics of solar cells. *Solar Energy*, 2011, 85.7: 1543-1550.
[26] GONG, Wenyin; CAI, Zhihua. Parameter extraction of solar cell models using repaired adaptive differential evolution. *Solar Energy*, 2013, 94: 209-220.
[27] APPELBAUM, J.; PELED, A. Parameters extraction of solar cells–A comparative examination of three methods. *Solar energy materials and solar cells*, 2014, 122: 164-173.
[28] BOUZIDI, K.; CHEGAAR, M. A. B. A.; BOUHEMADOU, A. Solar cells parameters evaluation considering the series and shunt resistance. *Solar Energy Materials and Solar Cells*, 2007, 91.18: 1647-1651.
[29] GHANI, Faisal; DUKE, Mike. Numerical determination of parasitic resistances of a solar cell using the Lambert W-function. *Solar Energy*, 2011, 85.9: 2386-2394.
[30] GUPTA, Deepak K., et al. Optimizing front metallization patterns: Efficiency with aesthetics in free-form solar cells. *Renewable energy*, 2016, 86: 1332-1339.
[31] FEMIA, Nicola, et al. *Power electronics and control techniques for maximum energy harvesting in photovoltaic systems*. CRC press, 2017.
[32] CUCE, Pınar Mert; CUCE, Erdem. A novel model of photovoltaic modules for parameter estimation and thermodynamic assessment. *International Journal of Low-Carbon Technologies*, 2012, 7.2: 159-165.
[33] Admin, “Draw a DC/DC boost converter in latex using CircuiTikZ,” TikZBlog, 26-Apr-2021. [Online]. Available: https://latexdraw.com/draw-a-dc-dc-boost-converter-in-latex-using-circuitikz/?fbclid=IwAR1c0N_vwHcj0Dr7albUSKUC0ZEcCGTA1ay76Ut8Hx67eXvnk5kd1yORfI4. [Accessed: 15-Dec-2021].
[34] GÓRECKI, Krzysztof; DETKA, Kalina. Influence of Power Losses in the Inductor Core on Characteristics of Selected DC–DC Converters. *Energies*, 2019, 12.10: 1991.
[35] KARIONGAN, Jakobus, et al. Optimization Of Renewable Energy Generation To Increase The Electrification Ratio In Borme District-Papua Province. *vol*, 14: 9.
[36] BAIMEL, Dmitry, et al. Improved fractional open circuit voltage MPPT methods for PV systems. *Electronics*, 2019, 8.3: 321.
[37] DHANDE, D. P.; CHAUDHARI, A. P.; MAHAJAN, G. K. A review of various MPPT techniques for photovoltaic systems. *Int. J. Innov. Eng. Res. Technol*, 2015, 2: 1-11.
[38] ERICKSON, Robert W.; MAKSIMOVIC, Dragan. *Fundamentals of power electronics*. Springer Science & Business Media, 2007.
[39] ASALIEH, Zakaria. High energy yield Bifacial-IBC solar cells enabled by poly-SiOx carrier selective passivating contacts. 2021.

[40] SolarEdge, "*Power optimizer efficiency: S-Series and P-Series*", November 2021. https://www.solaredge.com/sites/default/files/application_note_solaredge_optimizers_efficiency.pdf